

RIGA TECHNICAL UNIVERSITY
Faculty of Computer Science and Information Technology
Institute of Computer Control, Automation and Computer Engineering

Mihails KOVALOVS

PhD Student of Doctoral Study Programme “Image Processing and Computer Graphics,
Computer Engineering and Computer Networks”

**DEVELOPMENT OF METHODS AND ALGORITHMS FOR
BONE STRUCTURE RADIOLOGICAL IMAGE ANALYSIS
AND 3D VISUALIZATION**

Summary of the Doctoral Thesis

Supervisor
Dr. habil. sc. ing., Professor
A. GLAZS

RTU Press
Riga 2016

Kovalovs M. Bone Structure Analysis and Its 3D Visualization. Summary of the Doctoral Thesis. –R.: RTU Press, 2016. – 43 p.

Printed in accordance with the decision of the Council of the Institute of Computer Control, Automation and Computer Engineering, Faculty of Computer Science and Information Technology, Riga Technical University as of 12 November 2015, Minutes No. 12200-4.1/7.

**DOCTORAL THESIS PROPOSED TO RIGA TECHNICAL
UNIVERSITY FOR THE PROMOTION TO THE SCIENTIFIC DEGREE
OF DOCTOR OF ENGINEERING SCIENCES**

To be granted the scientific degree of Doctor of Engineering Sciences, the present Doctoral Thesis will be defended on 18 April 2016, at the Faculty of Computer Science and Information Technology, Riga Technical University, 1/3 Setas Street, Room 202.

OFFICIAL REVIEWERS:

Professor, *Dr. habil. sc. ing.* Janis Grundspenkis
Riga Technical University, Latvia

Professor, *Dr. habil. sc. ing.* Peteris Rivza
Latvia University of Agriculture, Latvia

Associate Professor, *Dr. sc. ing.* Vytenis Punys
Kaunas University of Technology, Lithuania

DECLARATION OF ACADEMIC INTEGRITY

I hereby declare that the Doctoral Thesis submitted for the review to Riga Technical University for the promotion to the scientific degree of Doctor of Engineering Sciences is my own and does not contain any unacknowledged material from any source. I confirm that this Thesis has not been submitted to any other university for the promotion to other scientific degree.

Mihails Kovalovs.....(Signature)

Date:

The Doctoral Thesis has been written in Latvian and includes introduction, 4 sections, conclusions, bibliography, and 4 appendices. It has been illustrated by 55 figures. The volume of the present Thesis is 118 pages, not including appendices. The bibliography contains 104 reference sources.

CONTENTS

1. GENERAL DESCRIPTION OF THE DOCTORAL THESIS.....	5
1.1. Topicality of the Research	5
1.2. The Aim and Tasks of the Doctoral Thesis.....	6
1.3. Thesis Statements.....	7
1.4. The Subject and Object of Research	7
1.5. The Methods of Research	7
1.6. Scientific Novelty of the Doctoral Thesis.....	7
1.7. Practical Significance of the Doctoral Thesis	7
1.8. The Structure of the Doctoral Thesis	9
2. CONTENTS OF THE DOCTORAL THESIS	9
2.1. Medical Imaging Techniques and Bone Structure	9
2.2. Medical Image Analysis and Visualization	10
2.3. The Proposed Bone Structure Radiological Image Analysis and Visualization Methods.....	11
2.3.1 Bone Structure Extraction	12
2.3.2 Bone Structure Analysis.....	18
2.3.3 Bone Structure Visualization.....	21
2.4. Approbation of the Medical Image Analysis and Visualization Methods	24
2.4.1 Input Data.....	24
2.4.2 Experiments.....	25
2.5. Results and Conclusions	35
3. REFERENCES	38

1. GENERAL DESCRIPTION OF THE DOCTORAL THESIS

1.1. Topicality of the Research

Bone structure analysis is needed to determine bone strength and assess the damage to the bone micro-architecture that appears due to such bone disease as osteoporosis. Obtaining data on static and dynamic properties of the human bone structure can result in a very large amount of information. Acquiring, processing and displaying this large amount of information present the most difficult challenges that exist for physicians and researchers. Modern information technologies allow solving this task by using computed tomography images and image processing methods.

Traditionally, during the medical image analysis, the radiologist performs a visual inspection of all the two-dimensional images that are divided into layers. Such radiological analysis is biased, because it is based on human perception and results in only qualitative assertions and judgments. Furthermore, medical images only allow viewing anatomical structures in a two-dimensional plane, for this reason, radiologists have to reconstruct the third dimension in their mind, while looking at the adjacent layers.

One of the most challenging sub-tasks of medical image analysis is the extraction of different tissues. This procedure is called image segmentation and it is a topical theme not only in the medical field, but also in many other sectors [1]–[11]. Physicians can perform this procedure manually on the computer screen. Manual extraction of a region of interest from the medical image takes more time when compared to a traditional or an automatic medical image analysis. Also, it requires additional software and experience, so typically it is not performed in clinical practice. In addition, such a manual analysis is very subjective, because it depends on human perception and produces variable measurements. To acquire more objective and reproducible measurements, it is necessary to perform the appropriate image processing methods and computational strategies. To speed up this process, it is desirable to develop fully automatic methods; however, the manual intervention often is necessary to correct the errors of an automated algorithm.

Medical image analysis is a topical issue; recently many new methods have been developed for various medical objects and tasks [12]–[15], as well as methods that are meant specifically for bone structure analysis and osteoporosis [16]–[20]. Most existing medical image processing algorithms are manual or semi-automatic algorithms. Such algorithms often require physicians to intervene in the medical image segmentation process, to set or edit the segmentation parameters, or manually outline the segments. Such operations require technical knowledge, which the physician might not have, and extra time, which is not desirable if the physician has to see many patients. Another disadvantage of the existing medical image segmentation methods is that they use images that were acquired using high resolution medical imaging devices that are not available in ordinary hospitals and diagnostic centres. It is therefore necessary to develop a completely automated bone structure segmentation algorithm that can work with images obtained by conventional computed tomography devices. The developed algorithm needs to be easy to use, so that it could be used by physicians without additional technical knowledge.

Modern information technologies can aid the diagnostic and surgery planning tasks. Medical image information can be visualized in three dimensions by creating a 3D model of the medical object. 3D models of the spine could be used in orthopaedic surgical planning, vertebral body osteoporotic or pathological fractures, in cases of spinal canal or intervertebral bone stenosis, vertebral arch and joint spur pathology.

The 3D model of the medical object is created on the basis of medical images (two-dimensional images) that are divided into layers; therefore, the visualization of a 3D model of the medical object can be separated into two stages. First, it is necessary to process all the medical images, to extract the bone structure regions or objects that are going to be visualized. This can be accomplished with segmentation methods. At this stage the necessity of a fully

automatic segmentation methods is most evident, since the number of medical images that are used in this process is quite large (from ten up to several hundred). Manually processing such a large number of images would require a considerable amount of time, so it is necessary to develop an automatic segmentation method that could extract all the bone structure regions from medical images.

At the second stage of visualization of the medical object, it is necessary to create the 3D surface of the extracted region. There are several algorithms that can deal with this task, in the medical field the most used method is volume rendering [21]–[24], where each voxel of the medical image is considered to be a separate object and is visualized accordingly. One of the disadvantages of volume rendering is that it requires a considerable amount of computational resources that are not available in most computers. Another visualization method is surface rendering [25]–[27], where the surface of the medical object is displayed with polygons. This method requires less computational resources but surface rendering has its own disadvantages. There are several methods, which can be used to create a polygonal surface. For example, triangulation algorithms [28]–[30] are meant for solid objects and they are unable to create a polygonal surface for porous objects, such as the cortical and the trabecular bone. Surface rendering methods that are based on the marching cube algorithm [31], [32] are able to create a polygonal surface for any object; however, the created surface has a distinct aliasing effect and the surface is not smooth. Thus, it is necessary to develop such a visualization algorithm that could be used to create a 3D model for objects such as the cortical and the trabecular bone. It is also necessary for the created surface to be of sufficiently good quality.

All the above-mentioned medical image processing methods are usually combined into one medical image processing system. There are several systems that contain various tools, which could be used for medical image processing and analysis. However, such systems are usually integrated into special workstations connected to the medical imaging equipment (computed tomography, magnetic resonance imaging, etc.). There are also systems that could be installed on any computer [3]; however, such systems, usually only allow viewing the medical images and do not contain the necessary medical image analysis tools. Therefore, to be able to accurately analyse the patient's medical images, physicians need to use medical workstations. However, it is not always possible, since they are occupied during a patient examination. Therefore, a necessity arises to develop a medical image processing and analysis system, which would contain the necessary image processing and analysis tools, and could be installed on any computer.

1.2. The Aim and Tasks of the Doctoral Thesis

The main aim of the Doctoral Thesis is to develop methods and algorithms that could be used for bone structure analysis and could automatically assess the changes in bone structure after a period of time. Such an analysis would be useful for physicians, so they could assess the effectiveness of treatment plant for patients with osteoporosis. All of the proposed methods should also be combined into a single medical image processing and analysis system, and this system must include the following abilities:

- to automatically extract the cortical and the trabecular bone from the medical image;
- to measure the average thickness of the cortical bone and the average density of the trabecular bone;
- to provide 3D visualization of the cortical and the trabecular bone.

In order to achieve the aim of the doctoral thesis, it is necessary to solve the following **tasks of the Doctoral Thesis**:

- to develop bone structure analysis methods, which would work with medical images that are stored in DICOM format;
- to develop methods for automatic extraction of bone structure (cortical and trabecular bone) from medical images;

- to develop methods for assessing the changes in bone structure;
- to develop methods for 3D visualization of bone structure.

1.3. Thesis Statements

- Automatic medical image processing methods could speed up the process of bone structure analysis and achieve reproducible measurements.
- Methods that could assess the changes in bone structure will be useful for physicians that need to assess the effectiveness of a treatment plan for patients with osteoporosis.
- 3D visualization of bone structure can aid the diagnostic and surgical planning tasks.

1.4. The Subject and Object of Research

The subject of research is methods and algorithms that are used to process the medical images of bone structure.

The object of research is sets of medical images of a human spine and legs that form the 3D structure of the bones. The images were acquired by means of computer tomography and were provided by Prof., Dr. med. A. Platkajis at Riga Stradins University.

1.5. The Methods of Research

The following image processing methods have been used in the Doctoral Thesis:

- Image segmentation;
- Region of interest extraction and analysis;
- 3D modelling and visualization.

1.6. Scientific Novelty of the Doctoral Thesis

New achievements are as follows:

1. Development of a fully automatic method for bone structure extraction from medical images that can work with the medical images of the human spine and legs.
2. Development of methods for assessing the changes in bone structure that will be useful for physicians who need to assess the effectiveness of a treatment plan for patients with osteoporosis. These methods can measure the average thickness of the cortical bone and the average density of the trabecular bone.
3. Development of a method for 3D visualization of bone structure. The proposed method can create 3D models of the cortical and the trabecular bone and it could visually show the thickness of the cortical bone. Compared with the existing method [33], the proposed method allows creating a visually smoother 3D surface.

1.7. Practical Significance of the Doctoral Thesis

The practical significance of the Doctoral Thesis is the developed medical image processing and analysis methods and algorithms that allow physicians to more effectively analyse the bone structure on medical images. The proposed algorithms can assess the changes in bone structure. This could help physicians assess the effectiveness of a treatment plan for patients with osteoporosis.

The results of the Doctoral Thesis have been presented in 11 scientific conferences and published in 11 scientific papers.

Publications:

1. Kovaļovs M., Glazs A. Medicīnisko objektu virsmu modelēšana, izmantojot triangulācijas un maršējošo kubu algoritmu // RTU zinātniskie raksti. 5. sēr., Datorzinātne. – 48. sēj. (2011), pp. 25–29.

2. Boločko K., Kovaļovs M., Glazs A. Medical Image 3D Visualization by Vector Based Methods // Multi Conference on Computer Science and Information Systems, Computer Graphics, Visualization, Computer Vision and Image Processing (IADIS): Proceedings, Italy, Rome, 24–26 July 2011, pp. 271–275. (Thompson ISI, EI Compendex).
3. Kovaļovs M., Glazs A. Medical Image Analysis to Determine the Effectiveness of Treating Osteoporosis // Scientific Journal of RTU Technologies of Computer Control, volume 13. – Riga: RTU, 2012, pp. 11–14 (EBSCOhost).
4. Kovaļovs M., Sisojevs A., Glazs A. A Surface Smoothing Method for a 3D Model of a Medical Object // International Symposium on Biomedical Engineering and Medical Physics (ISBEMP) 2012, pp. 74–77 (EBSCOhost, SpringerLink).
5. Sisojevs A., Kovaļovs M., Glazs A. Medical Object 3D Visualization Method Based on the Bézier Triangles // Multi Conference on Computer Science and Information Systems, Computer Graphics, Visualization, Computer Vision and Image Processing (IADIS) 2012, pp. 185–187 (Thompson ISI, EI Compendex).
6. Kovalovs M., Glazs, A. The Cortical and Trabecular Bone Extraction from Medical Images to Determine the Effectiveness of Treatment of Osteoporosis // Biomedical Engineering Conference Proceedings. Kaunas, Lithuania, 2012, pp. 103–106.
7. Kovalovs M., Platkajis A. Analysis of the Treatment Effectiveness for Osteoporosis by Using Images Acquired by Computer Tomography // Proceedings of the 9th Baltic–Bulgarian Conference on Bionics and Prosthetics, Biomechanics and Mechanics, Mechatronics and Robotics, Riga, Latvia, 17–21 June 2013, pp. 215–218.
8. Kovaļovs M., Glazs A., Trabecular Bone Segmentation by Using an Adaptive Contour // RTU Scientific Proceedings, Technologies of Computer Control. No.14, 2013, pp. 6–11 (EBSCO, ProQuest).
9. Kovalovs M., Glazs A., Automatic Medical Image Analysis for Measuring Cortical Bone Porosity // Biomedical Engineering Conference Proceedings. Kaunas University of Technology, Kaunas, Lithuania, 28–29 November 2013, pp. 87–90.
10. Kovaļovs M., Glazs A., 3D Visualization of Bone Structure and Thickness // RTU Scientific Proceedings, Technologies of Computer Control.. No.15, 2014, pp. 20–26 (EBSCO).
11. Kovalovs M., Glazs A., Automatic Medical Image Analysis for Measuring Bone Thickness and Density // Biomedical Engineering Conference Proceedings. Kaunas University of Technology, Kaunas, Lithuania, 27–28 November 2014, pp. 153–157.

Research Results Presented in Conferences:

1. The 52nd International Scientific Conference of RTU. Riga, 13–16 October 2011.
2. Multi Conference on Computer Science and Information Systems, Computer Graphics, Visualization, Computer Vision and Image Processing (IADIS), Italy, Rome, 24 –26 July 2011.
3. The 53rd International Scientific Conference of RTU dedicated to the 150th Anniversary of RTU, Riga, 10–12 October 2012.
4. International Symposium on Biomedical Engineering and Medical Physics (ISBEMP), Riga, 10–12 October 2012.
5. Multi Conference on Computer Science and Information Systems, Computer Graphics, Visualization, Computer Vision and Image Processing (IADIS). Lisbon, Portugal, 21–23 July 2012
6. Conference Biomedical Engineering. Kaunas, Lithuania, 25–26 October 2012.
7. International Conference on Bionics and Prosthetics, Biomechanics and Mechanics, Mechatronics and Robotics, Riga, Latvia, 17–21 June 2013.
8. The 54th International Scientific Conference of RTU. Riga, 14–16 October 2013.
9. Conference on Biomedical Engineering. Kaunas, Lithuania, 28–29 November 2013
10. The 55th International Scientific Conference of RTU. Riga, 14–17 October 2014.

1.8. The Structure of the Doctoral Thesis

The Doctoral Thesis consists of introduction, 4 chapters, conclusions, references and 4 appendices. The structure of the Doctoral Thesis can be described as follows:

Introduction — general description of the research. It describes the topicality of the research, sets the aim and tasks of the Doctoral Thesis, specifies the subject and object of the research, and underlines the scientific novelty and practical significance of the research.

The 1st Chapter: Medical Imaging Techniques and Bone Structure — describes three medical imaging techniques: computed tomography, magnetic resonance imaging and ultrasonography. A DICOM standard is also described, which is a medical image storing format. Bone structure and osteoporosis are also considered.

The 2nd Chapter: Medical Image Analysis and Visualization — describes the fundamental medical image segmentation and visualization methods.

The 3rd Chapter: The Proposed Bone Structure Radiological Image Analysis and Visualization Methods — describes the developed medical image processing and visualization methods, which are able to perform the following tasks: bone structure extraction, bone structure analysis and bone structure visualization.

The 4th Chapter: Approbation of the Medical Image Analysis and Visualization Methods — describes the experiments that were conducted using the developed methods.

Results and Conclusions of the Doctoral Thesis.

2. CONTENTS OF THE DOCTORAL THESIS

2.1. Medical Imaging Techniques and Bone Structure

Human body is a very complex system. Acquiring data about static and dynamic properties of a human body can result in a very large amount of information. Acquiring, processing and displaying this large amount of information present one of the most difficult tasks in medicine. One of the most effective ways of solving this task is to use medical images to display information about the human body [34].

Medical images are made using various imaging devices [38], but almost all medical imaging procedures come from one of the six major diagnostic procedures: planar, fluoroscopy, computed tomography, mammography, magnetic resonance, or ultrasound imaging [39], [40]. The first four modalities use x-rays; magnetic resonances are used by radio frequency radiation, while ultrasound imaging uses high-frequency sound waves.

Computed tomography is an imaging modality, which generates cross-sectional images that show the x-ray attenuation properties of the body. The cross-sectional image is generated based on the following procedure: X-rays are produced by an X-ray tube that are attenuated by the patient and measured by an X-ray detector. Using thin X-ray beams, a set of lines is scanned covering the entire field of view. This process is repeated for a large number of angles yielding line attenuation measurements for all possible angles and all possible distances from the centre. Based on all these measurements, the actual attenuation at each point of the scanned slice can be reconstructed [40].

One of the main advantages of computed tomography over conventional radiography is that in conventional radiography, subtle differences of less than about 5 percent in x-ray attenuation in the body are not visible in the image.

Magnetic resonance imaging measures the magnetic properties of the human body. Magnetic resonance imaging mainly focuses on the hydrogen atoms, because the human body contains a lot of this element, and it tries to visualize the tissues that contain hydrogen (bones, muscles, brains, fat etc.).

One of the main advantages of the magnetic resonance imaging is that it does not produce ionizing radiation. During a standard magnetic resonance procedure, the patient's body absorbs energy, but this energy is in the radio frequency portion of the electromagnetic spectrum and when it is absorbed by body tissues it causes heating, but not ionization.

The basic principle of ultrasound imaging is simple. A propagating wave partially reflects at the interface between different tissues. If these reflections are measured as a function of time, information is obtained on the position of the tissue if the velocity of the wave in the medium is known. Ultrasonography is a very popular modality, because it does not generate ionizing radiation. The benefits of using diagnostic ultrasound outweigh the risks that may be present.

The DICOM standard was developed in order to provide more medical imaging equipment interconnections. The DICOM standard describes file formats, medical directory structure, data communication protocols etc. At present, almost all imaging equipment and systems comply with the DICOM standard.

The bones can be divided into the two different types of structures: the trabecular (spongy) bone and cortical (compact) bone. Trabecular bone has a greater surface area than the cortical bone and it reconstructs faster. Trabecular bone is also known as spongy bone, because it resembles a sponge or honeycomb with many open spaces connected by flat planes of bone known as trabeculae. Cortical bone forms the outer shell of most bones.

Osteoporosis is the most common bone disease worldwide. Osteoporosis is characterised by the loss of bone mineral density and the deterioration of bone's micro architecture. As a result, bones become porous and brittle, which increases the risk of fractures from light injuries.

2.2. Medical Image Analysis and Visualization

Due to the increase of interest in medical imaging in clinical practice, as well as a large number of images obtained per patient, the workload of radiologists has significantly increased. For this reason, it becomes necessary to use information technologies for medical image analysis in order to help physicians and ease their workload.

Traditionally, during medical image analysis, a radiologist performs visual inspection of all two-dimensional images that are divided into layers. Such a radiological protocol is biased, because it is based on human perception and results in only qualitative assertions and judgments. Furthermore, medical images only allow viewing the anatomical structures in a two-dimensional plane, because of that, the radiologists have to reconstruct the third dimension in their mind, while looking at the adjacent layers.

One of the most challenging subtasks of automatic medical image analysis is the extraction of different tissues. This procedure is called image segmentation. This procedure can also be performed manually by a doctor on a computer screen, if the appropriate hardware and software are available. However, even if the appropriate equipment and programs are available, manual tissue region extraction from medical images, when compared to a traditional or automatic medical image analysis, is a time-consuming procedure and is usually not used in clinical practice.

The threshold segmentation is one of the simplest methods that can be used to divide an image into separate segments. By using a brightness threshold, it is possible to separate the image pixels into two classes: object pixels and background pixels. It is also possible to use several threshold values to split the image into several classes.

Region growing segmentation divides the image into several regions by grouping adjacent pixels with similar properties, such as brightness. This type of segmentation starts with a "seed" pixel, by determining the coordinates of the initial point from where the region grows, adding adjacent pixels with similar brightness. Later the created regions can be combined if the difference between their average brightness values is less than a specified threshold.

The contour extraction is similar to the region growing segmentation, except it does not group pixels, but looks for boundaries between regions. The boundaries are extracted using a local differential operator, which combines pixels that are most sensitive to the given operator. Ideally, when an image has a high contrast and no noise, this method can extract the boundaries between several different objects.

These image segmentation methods are rather simple, so using only these methods it is not always possible to extract the desired object from the medical image. Therefore, these methods are usually combined to create more complex methods for specific tasks [95].

Medical image information can be visualized in three dimensions, in order to help diagnose patients and plan surgical operations. Three-dimensional medical images are generated from three-dimensional voxel matrices that are obtained from sets of two-dimensional medical images. There are many methods that may be used to visualize medical image information; they can be separated into two groups: surface rendering and volume rendering.

To visualize the three-dimensional surface of a medical object, it is first necessary to extract this object from medical images. Not all medical object structures could be easily extracted from the image, but with bones it is possible because they have high contrast in images that were generated using computed tomography. The surface of an object can be displayed in several ways: a set of voxels, polygons or splines. In computer graphics, surface is usually displayed as a mesh of triangles. This way of displaying surfaces is very popular, because there are standardised software libraries that are based on using triangles to display surfaces.

Surface rendering requires image segmentation, which is a rather difficult task and does not always provide satisfactory results. Volume rendering allows overcoming this problem, by separately visualizing each voxel of a medical image, where each voxel has its own colour and transparency. Voxel has no geometric properties, except its location coordinates and voxels do not require textures. However, volume rendering requires considerably more computational power than software rendering, and also requires image segmentation to display complex medical object structures.

2.3. The Proposed Bone Structure Radiological Image Analysis and Visualization Methods

The goal of the Doctoral Thesis is to develop various medical image processing methods for automatic bone structure extraction, analysis and visualization. Medical images were acquired using computed tomography, which is available in most hospitals. It should be possible to combine all the proposed methods in one medical image processing system. To attain this goal, it is necessary to solve the following tasks:

- Opening and processing medical image files, which are stored using DICOM standard;
- Automatic extraction of bone structure;
 - Cortical bone extraction;
 - Trabecular bone extraction;
- Bone structure analysis;
 - Measurement of average thickness of cortical bone;
 - Measurement of cortical bone porosity;
 - Measurement of trabecular bone density;
- Bone structure visualization.

The procedure of opening the DICOM medical image files was developed based on publically available documentation of DICOM standard [65] that contains all the necessary information about data structures used in DICOM standard. Since DICOM is a universal medical image standard, the developed system can open and process most medical images that use the DICOM standard, not just those that were created using computed tomography.

The proposed methods can extract the bone structure from the medical images of human spine and legs. Since vertebrae and leg bones have different shapes, methods that are used in each case are also slightly different. The greatest difference appears in the cortical bone extraction, because the greatest visual difference between the spine and leg bones appears in the cortical bone. The trabecular bone extraction in both cases is mostly the same.

2.3.1 Bone Structure Extraction

One of the tasks of the Doctoral Thesis is to develop a fully automatic algorithm that does not require input from the user. This is necessary in order to ease and speed up the medical image analysis for the doctor, who will be working with these medical images. All parts of the algorithm work automatically without interruptions. However, a user still has the option to change main parameters of the algorithm, in order to increase the precision of the segmentation algorithm for a specific patient.

Bone structure extraction consists of five steps:

1. A medical image is divided into segments, which could possibly contain the cortical bone.
2. The segments are combined into clusters
3. The clusters are classified to find the cluster, which contains the cortical bone, and discard all other clusters.
4. A contour is created inside the cortical bone cluster, which adapts to the inner edges of the cortical bone.
5. The trabecular bone is extracted from the inside of the previously created contour.

The first three steps apply to the extraction of the cortical bone and the last two steps apply to the extraction of the trabecular bone. All steps of the bone structure extraction are described in detail in the following chapters. Various versions of the bone extraction algorithm have been published [96]–[98].

2.3.1.1 Cortical Bone Extraction

The proposed bone structure extraction algorithm starts with the cortical bone extraction. A medical image is divided into segments, which might contain the cortical bone. This step of the bone structure extraction is the same in both spine and leg bone cases.

The cortical bone extraction algorithm takes advantage of the property of medical images acquired with computed tomography, where each pixel contains the information about the tissue density. By taking advantage of this property, it is possible to extract the cortical bone from the image by setting a density threshold. The cortical bone density in medical images acquired with computed tomography is usually greater than 300Hu. Therefore, to extract the cortical bone it is possible to set the threshold value to 300Hu, and to find those pixels in the image with the density greater than the threshold.

In this case, the algorithm can be written as follows:

$$\begin{aligned} & \text{if } q_{i,j} \geq \delta, \text{ then } q_{i,j} \in A, \\ & \text{if } q_{i,j} < \delta, \text{ then } q_{i,j} \in B, \end{aligned} \tag{2.1}$$

where $q_{i,j}$ — density value of a pixel at (i,j) ;
 δ — set density threshold value (300 Hu);
 A — pixel group that could contain the cortical bone;
 B — pixel group that contains the background pixels;
 i,j — row and column number in the pixel matrix, $i,j \in [1:N]$;
 $N \times N$ — the size of the pixel matrix.

According to the proposed algorithm, the medical image is scanned by rows and those pixels with density greater than or equal to the threshold value δ are put in the pixel group A

(cortical bone), and those pixels whose density is less than δ are put in pixel group B (background).

However, there is one problem that may arise because of the porosity and holes, which appear in the cortical bone due to osteoporosis. This problem also affects the medical image processing, because the cortical bone may consist of several separate regions. Because of this, in the next step, when all pixels are combined into clusters some cortical bone pixels might be assigned to separate clusters and be lost. Therefore, it is necessary to reduce the threshold value to 100 Hu (Fig. 2.1b), and after the next step, when all the clusters are formed, reset the threshold value to 300 Hu.

There is also another serious problem — not all pixels with the density greater than 100 Hu or even 300 Hu contain the cortical bone. Figure 2.1b shows that after the cortical bone extraction, the images of legs still contain parts of the CT table and the images of vertebra contain parts of calcifications of the aortic wall. Therefore, in the next steps of the algorithm, it is necessary to clean up the image from all pixels that do not contain the cortical bone.

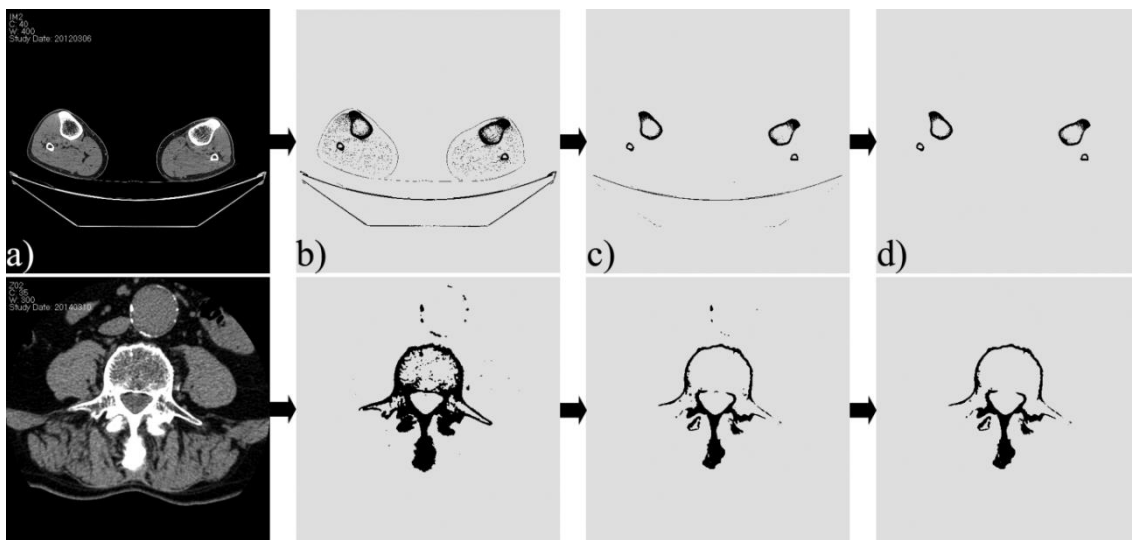


Fig. 2.1. Cortical bone extraction from leg (upper row) and spine (bottom row) medical images

a) original medical images, b) images after segmentation, with threshold set to 100 Hu, c) images after segment clustering, d) images after cluster classification.

2.3.1.2 Segment Clustering

Segment clustering takes all the pixels extracted in the previous step and combines them into clusters. The clustering process is based on a region growing algorithm [91]. Taking into account formula (2.1), the clustering algorithm is described in the following way:

1. The image is scanned horizontally and the pixels that belong to the pixel group B (background) are assigned to the 0 cluster.
2. The image is scanned horizontally and if a pixel belonging to pixel group A and not assigned to any cluster is found, then this pixel is assigned to a new (current) cluster and it becomes a starting point.
3. All neighbouring pixels around the starting point are analysed.
4. If among the neighbouring pixels, there are pixels that are not assigned to any cluster, then these pixels are assigned to the current cluster and they become new starting points, the 3rd and 4th steps are repeated until all starting points and their neighbouring pixels have been analysed.
5. The 2nd step is repeated (to find the next pixel that belongs to pixel group A and is not assigned to any cluster), and then the 3rd and 4th steps are also repeated (with a new starting point) until all image pixels are assigned to a cluster.
6. The pixels with a density less than 300 Hu are discarded.

2.3.1.3 Cluster Classification

In this step, all of the previously created clusters are classified to find those clusters that contain the cortical bone and discard all other clusters. Before the classification begins, all very small clusters that could not contain the cortical bone are discarded. This is done based on how many pixels are assigned to a given cluster. If a cluster consists of less than 50 pixels, then this cluster and all of its pixels are discarded.

During the cluster classification, the significant differences start to appear between the vertebra and leg bone image processing algorithms. This happens mainly because, in each individual case it is necessary to find a different number of clusters: in the case of the vertebra it necessary to find only one cluster, but in the case of leg bones it necessary to find two or four clusters.

In the case of leg bone images, the cluster classification is significantly more complex, because from all previously created clusters it is necessary to find those two or four clusters, which contain the cortical bone. To find these clusters, all clusters are analysed in pairs in order to find such a pair where both clusters have three similar property values: size, position and proportion.

The size of a cluster is calculated as a number of pixels that are assigned to this cluster. The position of the cluster is the centre coordinate of this cluster. The proportion of cluster is calculated as a width of the square (that describes the cluster) divided by its height.

In the cluster pair analysis process, all possible combinations of cluster pairs are looked at to find such a pair that fulfils three requirements:

1. The size requirement is fulfilled if the difference between the cluster sizes (P) is less than 25 % of the average size of both clusters.

$$P_1 - P_2 < 0.25 * \left(\frac{P_1 + P_2}{2} \right), \quad (2.2)$$

where P_1 — number of pixels assigned to the first cluster;
 P_2 — number of pixels assigned to the second cluster.

2. The position requirement is fulfilled if the distance between the cluster centre points c_1 and c_2 on y axis is less than 10 % of the height of the medical image (this distance is marked with letter a in Fig. 2.2).

$$c_1 - c_2 < 0.1 * M, \quad (2.3)$$

where c_1 — centre point coordinates of the first cluster on the y axis;
 c_2 — centre point coordinates of the second cluster on the y axis;
 M — height of the medical image (total number of pixels along the y axis).

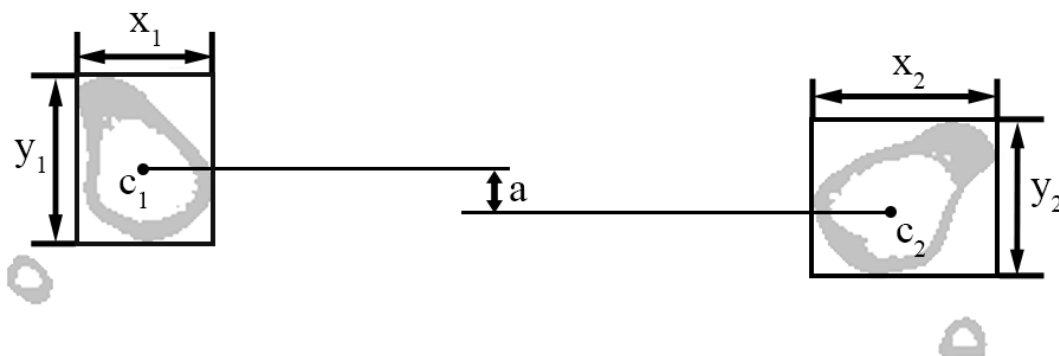


Fig. 2.2. Leg bone cluster properties that are calculated using formulas (2.2), (2.3) and (2.4).

3. The proportion requirement is fulfilled if the proportion value of both clusters is greater than 0.5 and less than 1.7.

$$0.5 < \frac{x_i}{y_i} < 1.7, \quad i \in [1:2] \quad (2.4)$$

where x_i — width of the cluster i ;
 y_i — height of the cluster i .

In the case of vertebra images, cluster classification is considerably simpler than with leg bone images, because here it is necessary to find only one cluster which usually is located at the centre of the image. This cluster can be easily distinguished from all the others, because it is the largest cluster that is closest to centre of the medical image. The algorithm can be described as follows:

1. The centre point coordinates are calculated for each cluster.
2. The distances from each cluster centre point to the medical image centre are measured.
3. Cluster with the shortest distance is classified as a vertebra cluster.
4. All other clusters are discarded.

After the cluster classification, only the clusters that contain the cortical bone remain on the medical image, thus defining the pixels of the cortical bone. Later these clusters or pixels can be used for bone structure analysis to measure the thickness or the porosity of the cortical bone; these pixels can also be used for the visualization of the cortical bone or for the extraction of the trabecular bone.

2.3.1.4 Creation of an Adaptive Contour

With this step the trabecular bone extraction begins by creating a contour inside the previously extracted cortical bone. This contour adapts to the inner edge of the cortical bone, which is used to extract the trabecular bone that is located inside the cortical bone.

Such a contour is necessary, because it is not always possible to extract the trabecular bone using only algorithms that are based on region growing. This mainly happens, because there might be holes in the cortical bone and a region growing algorithm might “spill” outside of the cortical bone. Therefore, it is necessary to create a contour that adapts to the edges of the cortical bone and ignores the holes. The developed algorithm for creation of an adaptive contour has been published [99].

Before the adaptive contour can be created, a general cortical bone contour is created, which will be used to set boundaries for the adaptive contour. This general contour is created by highlighting pixels where the tissue density changes a value from positive to negative. Then from all the created contours, the smaller ones that consist of less than 100 pixels are discarded. As can be seen in Fig. 2.3, the created contours describe more than just the cortical bone, but this is considered acceptable, since this contour will only be used to restrict the adaptive contour.

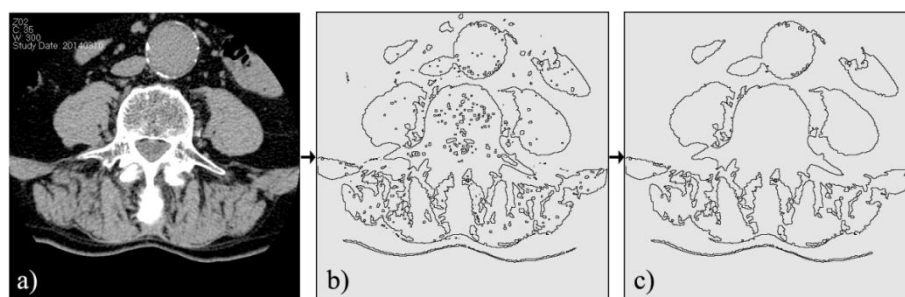


Fig. 2.3. The creation of the general cortical bone contour

a) original medical image, b) the created contours, c) smaller contours are discarded.

To create the adaptive contour, a starting point is selected that is located inside the cortical bone area. The starting point selection algorithms are different for the vertebra and leg bones, because they have a different shape of the cortical bone.

In the case of leg bone images, the starting point selection algorithm is rather simple, because the cortical bones of legs have a round shape and the starting point can be selected as a centre of the cortical bone. Therefore, the starting point selection algorithm for leg bone images can be described as follows:

1. Find the minimal (x_{min}) and maximal (x_{max}) coordinates of cortical bone on the x axis.
2. Find the minimal (y_{min}) and maximal (y_{max}) coordinates of cortical bone on the y axis.
3. Calculate the coordinates of the starting point (x_{sp}, y_{sp}), as the average of the minimum and maximum values along the x and y axes (Fig. 2.4a)

$$x_{sp} = \frac{x_{min} + x_{max}}{2} \quad (2.5)$$

$$y_{sp} = \frac{y_{min} + y_{max}}{2} \quad (2.6)$$

where x_{sp}, y_{sp} — starting point coordinates;

x_{min}, x_{max} — minimal and maximal coordinates of cortical bone on the x axis;

y_{min}, y_{max} — minimal and maximal coordinates of cortical bone on the y axis.

In the case of vertebra images, the starting point selection algorithm is more complex, than in the case of leg bones, because the shape of the cortical bone is very different and the centre of the vertebra cannot be considered a starting point, since it is usually located on the cortical bone or outside of it. Therefore, the selection of a starting point for vertebra images is a longer process (Fig. 2.4b) and it consists of the following steps:

1. The coordinates for a rectangle (that describes the cortical bone) are calculated, the selection of a starting point is limited to the upper half of this rectangle.
2. The starting point y coordinate is selected as the centre y coordinate of the upper half of the rectangle.
3. The average coordinates for the left and right edges of the cortical bone are calculated.
4. The starting point x coordinate is selected as the middle point between the previously calculated left and right edge of the cortical bone.

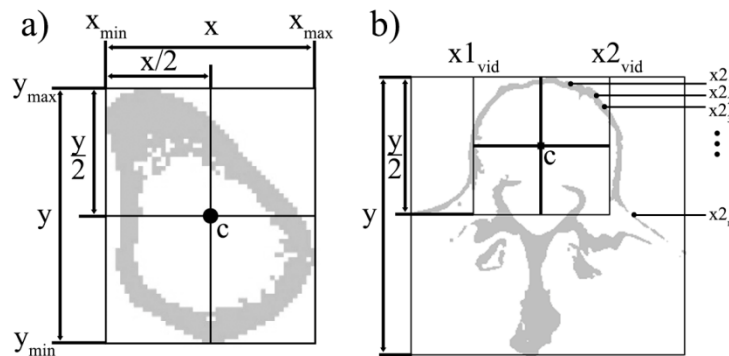


Fig. 2.4. Starting point selection

a) the case of leg bones, b) the case of vertebra.

After the starting point is selected, the creation of the adaptive contour is the same for both the leg bones and vertebra. The main idea of the adaptive contour creation algorithm is that the control points are placed at the starting point and then these control points move in all directions until they reach the cortical bone, thus adapting to the edges of the bone. This algorithm consists of the following steps:

1. Four control points are placed at the starting point and all control points are assigned movement vectors with the length — 1 and four basic directions: $(1,0), (-1,0), (0,1), (0,-1)$ (Fig. 2.5a).
2. Each control point that is not in a “stopped” state moves over one pixel in the direction of its vector. The control point is set to a “stopped” state, if after moving it is located on the cortical bone or the general cortical bone contour (Fig. 2.5c).
3. If the distance between any two neighbouring control points becomes greater than 10 pixels, then a new control point is created between them with a new movement vector that is equal to the normalized sum of both neighbouring control points (Fig. 2.5b). A new control point is not created if any of the neighbouring control points is in a “stopped” state.
4. The second and third steps are repeated, until all control points are in a “stopped” state.
5. The distances between all neighbouring control points are measured to find the control points that are outside of the cortical bone. The control points that have a distance value greater than 20 pixels are marked (Fig. 2.5d).
6. All control points that are located between two consecutive marked control points are discarded (Fig. 2.5e).

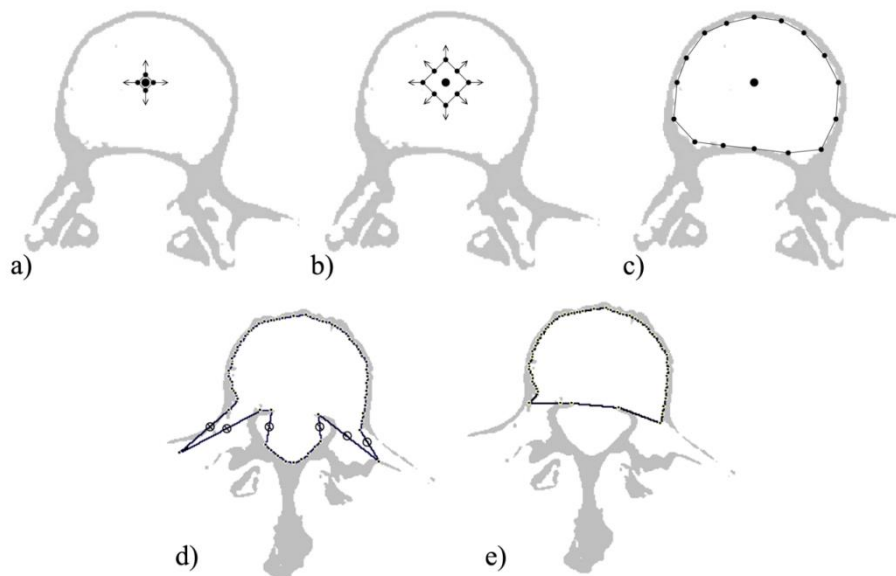


Fig. 2.5. The adaptive contour creation

a) control points are placed at the starting point, b) new control points are inserted, c) control points have stopped at the cortical bone, d) control points, which are outside of the cortical bone, are marked, e) the created contour after discarding the outer control points.

2.3.1.5 Trabecular Bone Extraction

The trabecular bone extraction is the last step in extracting the bone structure from a medical image. In this step, the Laplace filter is used to extract the trabecular bone from inside of the contour that was created in the previous step. This step is almost the same for both the vertebra and leg bone images; the only difference is that it needs to be repeated for each bone in the case of leg bone images. The trabecular bone extraction algorithm consists of the following steps:

1. The Laplace filter is applied to the original medical image, this filter highlights the transitions between different tissues and assigns a value to each pixel from a range of 0 to 255 (Fig. 2.6b and Fig 2.6c).
2. All pixels, which are located inside of the previously created contour, are selected. This is done using the region growing algorithm that was used in the segment clustering step (Fig. 2.6d).

3. The pixels with an assigned value greater than 25 (10 % of the maximum value) are discarded (Fig. 2.6e).

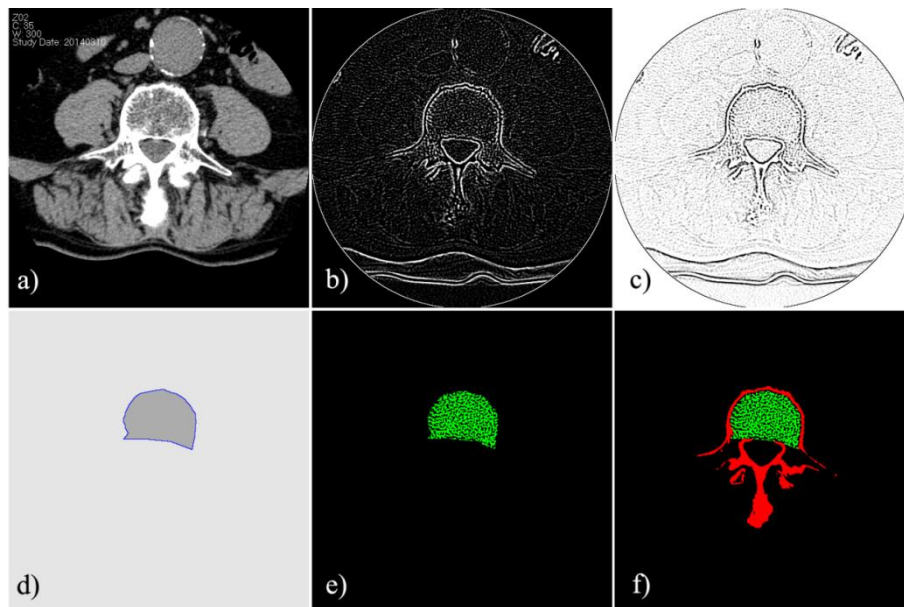


Fig. 2.6. Trabecular bone extraction

a) original medical image, b) Laplace filter is applied to the image, c) inverted Laplace filter is applied to the image, d) contour that was created in the previous step, e) extracted trabecular bone, f) final image that contains the extracted cortical and trabecular bone.

2.3.2 Bone Structure Analysis

The main goal of bone structure analysis is to measure the changes in bone structure over a period of time. This is useful for patients with osteoporosis, whose bone structure deteriorates over time and it is necessary to determine the rate of deterioration and evaluate the effectiveness of treatment.

The changes in bone structure are measured by analysing two sets of medical images. One set of images should be made at the beginning of treatment and the second set of images should be made after a certain period of time. The effectiveness of treatment of osteoporosis is evaluated by analysing these three bone structure measurements:

- Average thickness of the cortical bone.
- Cortical bone porosity.
- Average density of the trabecular bone.

To automatically measure these three parameters, it is first necessary to extract the cortical and trabecular bone from the medical images, which was described in the previous chapters.

2.3.2.1 Measuring the Average Thickness and Porosity of the Cortical Bone

The average thickness and porosity of the cortical bone are measured using the inner and outer contour of the cortical bone. The creation of the inner contour was described in the previous chapter. The outer contour is created from the inner contour. The outer contour creation algorithm consists of the following steps:

1. The outer contour is created as a copy of the inner contour. Each control point of the outer contour is assigned a vector, which is calculated as a normal vector of this control point.
2. The outer contour expands, control points move in direction of their vectors until all control points are located outside of the cortical bone (Fig. 2.7a).

3. The outer contour shrinks, control points move in the opposite direction of their vectors until all control points are located on the outer edge of the cortical bone (Fig. 2.7.b).
4. To better describe the shape of the cortical bone, new control points are inserted into the outer contour, they are placed in the middle between the existing control points. Each new control point is assigned a vector, which is calculated as a normal vector of this control point (Fig. 2.7c).
5. New control points move in the direction of their vectors, until all control points are located on the outer edge of the cortical bone (Fig. 2.7d).

The average thickness of the cortical bone is measured as an average distance between the control points of the inner and outer contours. The new control points that were created in the 4th step are ignored since they do not have a corresponding control point on the inner contour (Fig. 2.7e).

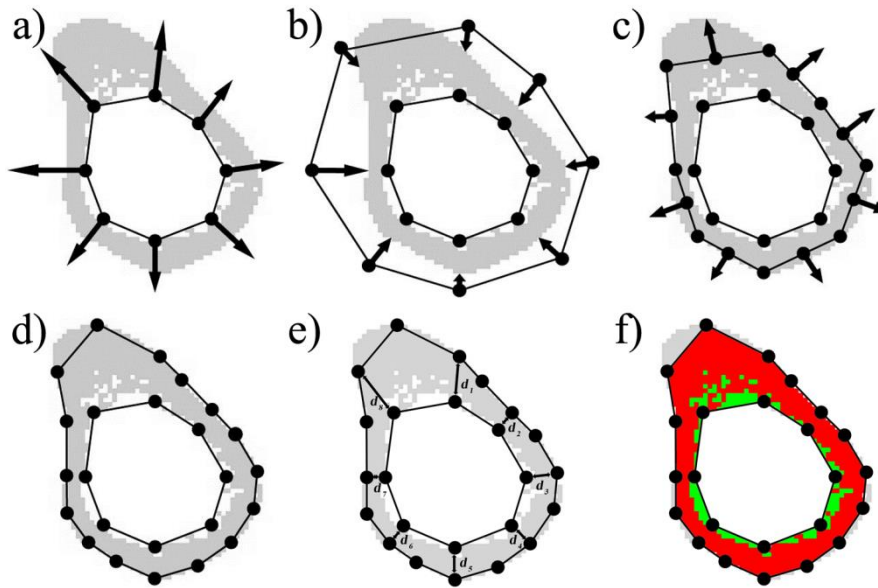


Fig. 2.7. The creation of the outer contour of the cortical bone and the measurement of average thickness and porosity

a) the outer contour is created as a copy of the inner contour, and afterwards it expands, b) the outer contour shrinks, c) new control points are inserted into the outer contour, afterwards they expand, d) the created outer contour of the cortical bone, e) average thickness measurement, f) porosity measurement.

The average thickness (T_{avg}) of the cortical bone is calculated using the following formula:

$$T_{avg} = \frac{1}{n} \sum_{i=1}^n d_i, \quad (2.7)$$

where T_{avg} — the average thickness of the cortical bone, pixels;
 d_i — the distance between a control point on the inner and outer contour, pixels;
 n — the number of control points in the inner contour.

In the case of medical images of the vertebra, it is only necessary to measure the upper part of the cortical bone, where the control point vector's y value is positive. This is done because the bottom part of the vertebra's cortical bone contains growth (spinous and transverse process) that does not affect the average thickness of the cortical bone.

The porosity of the cortical bone is measured between the inner and outer contours, by comparing the number of pixels that belong to the cortical bone with the total number of pixels

that are located between the contours. The porosity measurement can be seen in Fig. 2.7f, where the pixels that belong to the cortical bone have a red colour and the other pixels have the green colour. The porosity measurement is calculated by the following formula:

$$P = \frac{k}{v} \cdot 100, \quad (2.8)$$

where P — porosity value as a percentage;

k — number of pixels between the inner and outer contour that do not belong to the cortical bone;

v — total number of pixels between the inner and outer contour.

The developed cortical bone porosity and average thickness measurement algorithms have been published [100], [101].

2.3.2.2 Measuring the Average Density of the Trabecular Bone

To obtain more accurate measurements of trabecular bone density, only a small region of the trabecular bone is analysed and the size of this region does not change between multiple different images. This is necessary, because the contours that are created by the automatic trabecular bone extraction algorithm are not identical on all the different images.

This region is determined, first by finding the centre point (C) of the trabecular bone (Fig. 2.8a). The coordinates of this point are calculated as an average value of all the control point coordinates of the inner contour. Then a window-square is placed at the centre point coordinates (Fig. 2.8b). The average density of the trabecular bone is measured inside this square.

The average density of the trabecular bone is measured as a pixel ratio, by dividing the number of pixels that belong to the trabecular bone (in Fig. 2.8b they are coloured yellow), with the number of all other pixels that are located inside of the square region. The average density (D_{avg}) of the trabecular bone is calculated by the following formula:

$$D_{avg} = \frac{t}{p}, \quad (2.9)$$

where D_{avg} — the average density of the trabecular bone;

t — the number of pixels inside of the square that belong to the trabecular bone;

p — the number of all other pixels inside of the square.

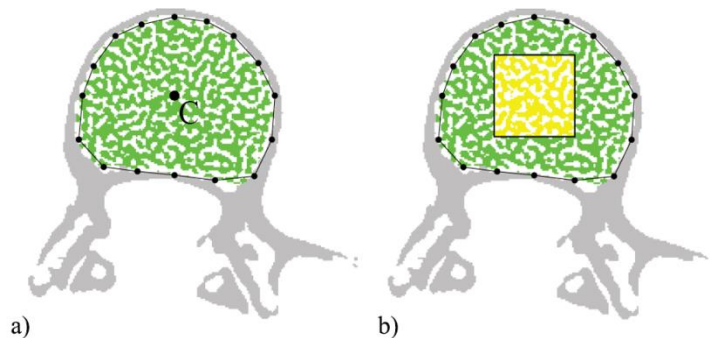


Fig. 2.8. Measuring the average density of the trabecular bone

a) the centre point of the trabecular bone, b) measurement square.

2.3.3 Bone Structure Visualization

Three-dimensional visualization of bone structure or any other medical object is an important aspect of medical image analysis and studies. The analysis and visualization of medical images that were acquired by computed tomography or magnetic resonance imaging are useful in medical research and clinical practice. The ability to visualize the structure, orientation, position and size of a medical object is very useful to scientists and doctors.

To create the three-dimensional model of a medical object, it is first necessary to process the medical images in order to extract the object of interest from the medical image. After that, several methods can be used to create the three-dimensional model of a medical object. At first, it was attempted to use the triangulation method [28], [29], [102] for creating the 3D model of bone structure. However, to correctly use the triangulation algorithm, it is necessary that the extracted object would not have any holes and could be described with one closed contour on every medical image. Then the triangulation algorithm would be able to create 3D surface of the object, by connecting the closest control points on the contours with triangles (Fig. 2.9).

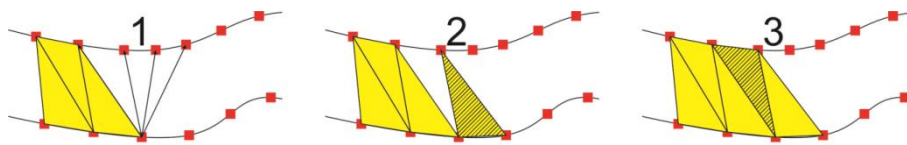


Fig. 2.9. Triangles are created between two contours.

The cortical and trabecular bones have a complex structure that might contain various holes and disconnected parts; therefore, it is impossible to describe it with one closed contour. In this case, the triangulation algorithm cannot create the surface of a 3D model. When a contour has holes in it or the medical object is described with several contours on a single medical image, the triangulation algorithm cannot correctly choose which control points to connect (Fig. 2.10).

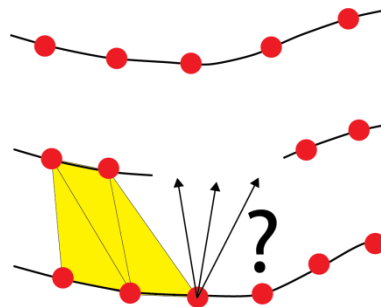


Fig. 2.10. Triangulation algorithm cannot choose the control points.

Therefore, this Doctoral Thesis uses the marching cube algorithm to create the model of a medical object. Marching cube algorithm could be used to create the 3D model of complex structures that the triangulation algorithm cannot work with [102].

One of the main disadvantages of the marching cube algorithm is that the models that are created using this algorithm have a distinct staircase effect between the layers of medical images, which can be seen on Fig. 2.11c. Therefore, to obtain a better quality model, a three-dimensional surface smoothing algorithm has been developed in this Doctoral Thesis.

The surface of a 3D model is described with vertices that are connected into triangles. The main idea of the smoothing algorithm is to change the position of vertices, in order to smooth out the sharp edges that might appear between the triangles. The smoothing algorithm consists of the following steps:

1. All vertices of the model are sequentially analysed.

2. All vertices that are connected to the currently analysed vertex are found.
3. The new coordinates are calculated for the current vertex as average coordinates of all the vertices that are connected to the current vertex.
4. A new vertex is created with the coordinates that were calculated in the previous step.
5. The first four steps are repeated for all vertices.
6. A new model is created using all new vertices, applying the same connections between the vertices of the original model.

The smoothing algorithm is visually shown in Figs. 2.11a and 2.11b. Figure 2.11c shows the model that was created using the marching cube algorithm, and Fig. 2.11d shows the same model after the smoothing algorithm was applied to it. The developed smoothing algorithm has been published [30].

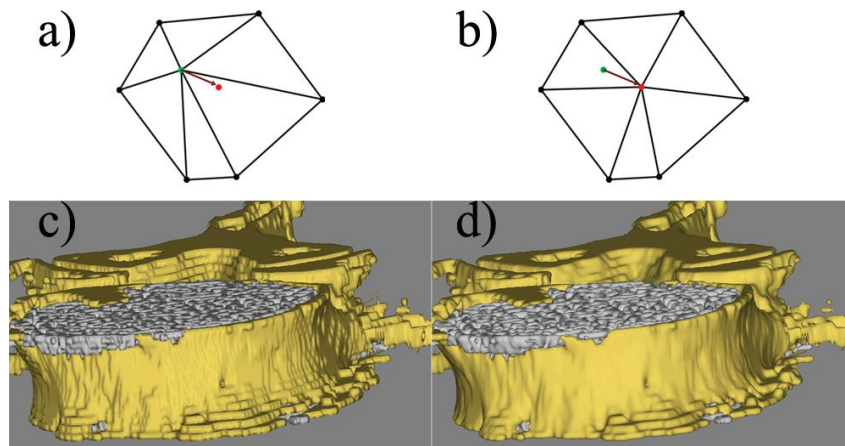


Fig. 2.11. The smoothing algorithm and the created models

a) The original model vertex (green) is moved to a new location (red), b) the connections between the vertices are preserved, c) three-dimensional model of a vertebra that was created using the marching cube algorithm, d) the same model with a smoothed surface.

2.3.3.1 Cortical Bone Thickness Visualization

Cortical bone thickness visualization allows showing the thickness of the bone in three dimensions, which could help physicians determine the condition of the bone. Before the three-dimensional thickness model can be created, it is necessary to process the medical images in order to create the cortical bone thickness map.

The first step in creating the bone thickness map is to apply the distance transform function [103] on the medical image with the extracted cortical bone. The distance transform function assigns a value to each pixel of the cortical bone. This value is equal to the distance from the current pixel to the closest pixel that does not belong to the cortical bone (background). The simplified example of the distance transform function can be seen in Fig. 2.12.

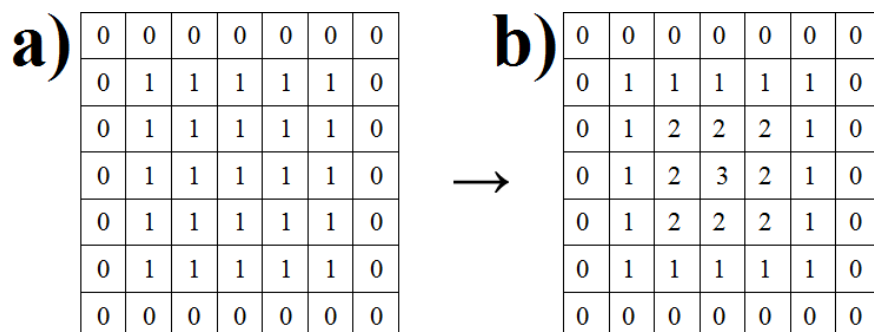


Fig. 2.12. Distance transform function example

a) The medical image is described with numbers, where 0 indicates the background pixel and 1 indicates the cortical bone pixel, b) the result of applying the distance transform function.

Figure 2.13a shows the result of applying the distance transform function to a real medical image of a vertebra, where the brightness of a pixel represents the distance from the pixel to the background (higher brightness means greater distance).

Using the distance transform function creates the distance map, where each pixel of the cortical bone is assigned a distance value. The cortical bone pixels were extracted from the image using a method that was described in the previous chapters (Chapter 2.3.1). The distance map is used to create the cortical bone thickness map. The algorithm of creating the thickness map consists of the following steps:

1. The image is scanned horizontally looking for a cortical bone pixel that is not assigned a thickness value and has at least one neighbouring background pixel. The found pixel becomes the current pixel.
2. A search radius is set to 1 pixel; the algorithm looks for pixels around the current pixel, inside of the search radius, with the largest distance value in the distance map.
3. Search radius is increased by 1 pixel and the algorithm again searches for the pixels around the current pixels with the largest distance value inside of the search radius.
4. If in the previous step a pixel is found with a greater distance value than in the previous steps, then the third step is repeated, otherwise the current pixel is assigned a thickness value that is equal to the search radius.
5. First four steps are repeated, until all cortical bone pixels that are located next to the background are assigned a thickness value.
6. The image is scanned horizontally looking for a cortical bone pixel that has at least one neighbouring pixel with an assigned thickness value.
7. Each pixel that is found in the previous step is assigned a thickness value that is equal to the average thickness of all its neighbouring pixels.
8. The sixth and seventh steps are repeated, until all cortical bone pixels are assigned a thickness value.

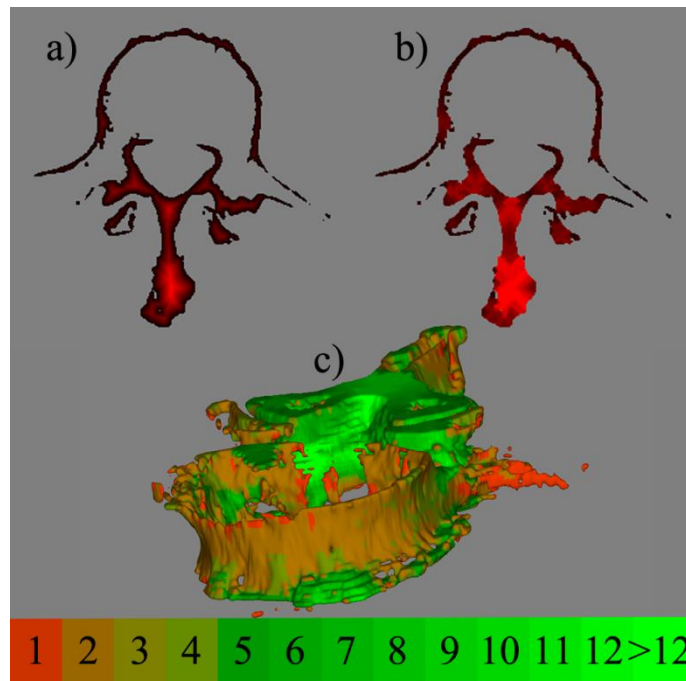


Fig. 2.13. Examples of the distance and thickness maps and the created thickness model

a) an example of the cortical bone distance map, b) an example of the cortical bone thickness map, c) three-dimensional model of a vertebra, showing the thickness of the cortical bone with different colours, at the bottom there is a thickness colour scale in pixels.

An example of a created thickness map can be seen in Fig. 2.13b. This thickness map is then implemented into the marching cube algorithm, which is used to create the three-dimensional model of the cortical bone.

When the three-dimensional model of the bone is created, each marching cube assesses the thickness values of pixels that are inside of this cube. Each cube is assigned a thickness value that is equal to the average thickness of all the pixels that are inside of this cube. When, the three-dimensional surface is created inside of the marching cubes, each polygon is assigned a thickness value of its marching cube. During the visualization, each polygon is drawn with different colours, depending on the polygon thickness values. Figure 2.13c shows a three-dimensional model of a vertebra, where each polygon displays the thickness of the cortical bone with different colours. At the bottom of the image, there is a colour scale, which shows what thickness each colour represents. The developed cortical bone thickness visualization algorithm has been published [104].

2.4. Approbation of the Medical Image Analysis and Visualization Methods

All the proposed methods have been developed using Delphi programming language and are combined in one medical image processing program. This program has been used to conduct various experiments with the developed methods. The graphical user interface of the developed program can be seen in Fig. 2.14.

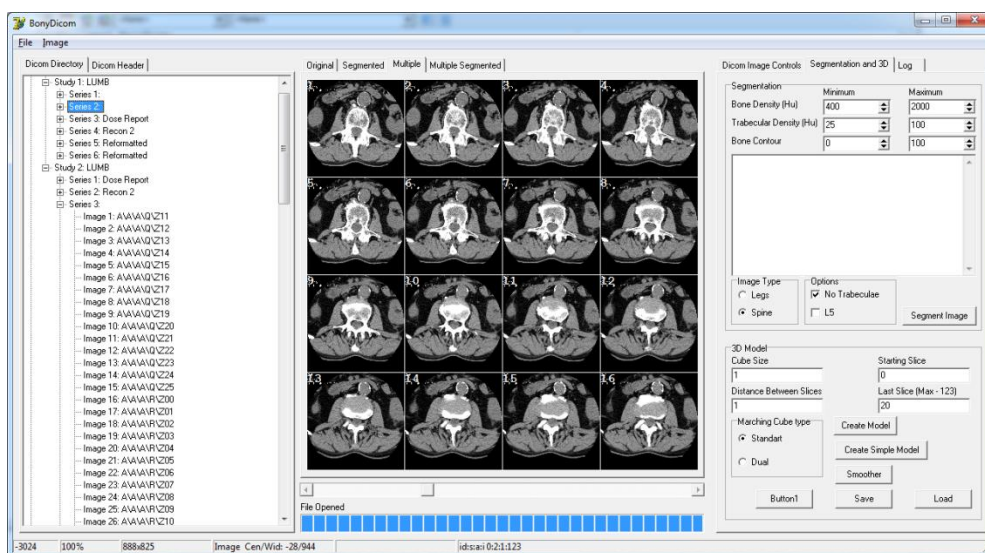


Fig. 2.14. The graphical user interface of the developed medical image processing program.

Various experiments have been conducted in the Doctoral Thesis to test the effectiveness of the proposed bone structure analysis and visualization methods. The experiments have been conducted with the following methods:

- The extraction of bone structure from medical images.
- Measurement of changes in bone structure.
- Bone structure visualization.

2.4.1 Input Data

The input data used in the experiments are the medical images of the spine of real patients, which are stored in the DICOM format, and they were acquired using computed tomography (medical images were provided by Assoc. prof. of Riga Stradins university, Dr. med. A. Platkais). Medical images that were acquired using the computed tomography or magnetic resonance imaging display the human bone structure in layers. Depending on the layer (medical image) thickness and the purpose of the medical examination, the computed tomography might generate several hundred images for one patient. The experiments in this

Doctoral Thesis used the medical images of the human spine. Typical set of medical images of the spine might consist of 50 to 150 medical images.

In radiology, the bone structure analysis usually focuses on the fourth L4 and fifth L5 vertebra of the lumbar spine (Fig. 2.15). Therefore, most experiments were focused on one specific vertebra — the fourth L4 lumbar vertebrae. The medical images of the L4 vertebrae of one patient can contain from 9 up to 15 medical images.

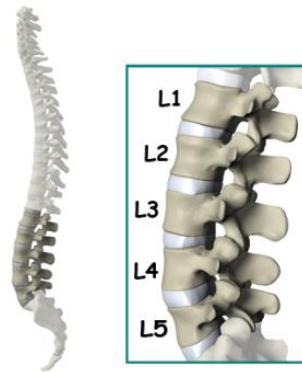


Fig. 2.15. The human spine and the lumbar spine.

The medical images of 35 patients were used in the Doctoral Thesis. One experiment used two different sets of medical images of 15 patients that were made at different times. Figure 2.16 demonstrates the medical images of the L4 vertebrae of one patient that show the bone structure of the vertebrae in layers.

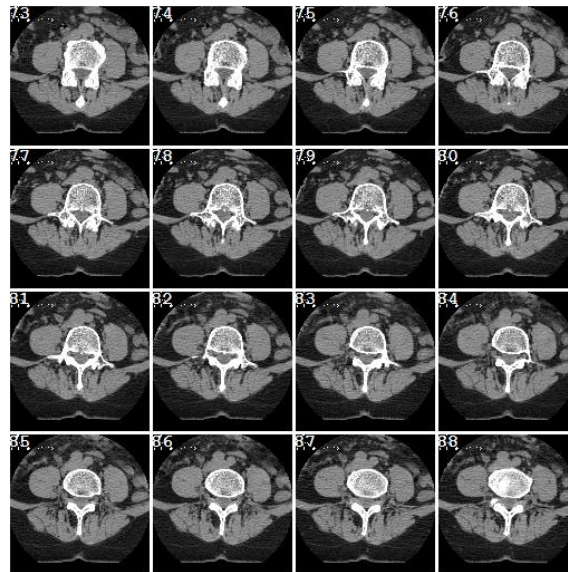


Fig. 2.16. Medical images of L4 vertebra of one patient.

2.4.2 Experiments

Experiments have been conducted with all the developed algorithms. It was important to test whether these algorithms were capable of extracting the bone structure from medical images and if they could be used to evaluate the changes in bone structure. The developed methods were also tested to see if they could be used to create and display the 3D models of the bone structure. Therefore, the experiments can be divided according to three tasks:

1. To test the developed algorithms to see if they can extract the cortical and trabecular bones from the medical images, and if they can measure the average thickness of the cortical bone and the average density of the trabecular bone. To check if it is possible to

- classify the healthy patients and the ones with osteoporosis based on their bone structure measurements.
2. To test the developed algorithms to see if they can be used to evaluate the changes in bone structure in patients with osteoporosis. To evaluate the possibility of using the algorithms to determine the effectiveness of osteoporosis treatment plan based on changes in bone structure after a certain time period.
 3. To test the developed algorithms to see if they can create and display the 3D models of the spine and vertebra. To compare the results with an existing medical image processing system 3D-Doctor [33].

2.4.2.1 Cortical and Trabecular Bone Structure Extraction

The developed bone structure extraction algorithm was used to extract the cortical and trabecular bone from the medical images. The algorithm was tested on sets of medical images from two patient groups. The first group consisted of eight healthy patients aged 18 to 26 years, and the second group consisted of six patients with osteoporosis aged 55 to 86 years. The average thickness of the cortical bone and the average density of the trabecular bone were measured in all patients in order to verify that the proposed algorithm could be used to distinguish the healthy patients from patients with osteoporosis based on their measurements.

Input data: Medical images (that are stored in DICOM format) of L4 vertebra of eight healthy patients and six patients with osteoporosis (187 images in total). The number of layers (images) for each patient was selected from 9 to 15 depending on the size of the vertebra.

Tasks:

1. To extract the cortical and the trabecular bone from the medical images.
2. To measure the average thickness of the cortical bone and the average density of the trabecular bone.
3. To compare the results between the two groups of patients in order to determine whether patients can be distinguished by their bone structure measurements.

Before the extraction of the bone structure can begin, it is necessary to choose the value of the cortical bone density threshold. This threshold is used in the first step of the bone extraction algorithm to find the pixels that might contain the cortical bone on the medical image. The cortical bone threshold value is the only parameter that is set by the user. However, that is not always necessary, since it is usually assumed that the cortical bone density of healthy people is greater than 300 Hu. For people suffering from osteoporosis, cortical bone density is considerably lower. Therefore, in order to compare both patient groups, it is necessary to select the cortical bone threshold value that would suit both groups.

To select the appropriate threshold value, the developed bone extraction algorithm was applied to several medical images from both patient groups, using different threshold values. An example of the extracted bone structures can be seen in Fig. 2.17.

Several threshold values were considered: from 250 Hu up to 350 Hu. For healthy patients the 250 Hu threshold was too small, because using this threshold value, the cortical bone was not accurately extracted. Several objects, inside of the cortical bone, were incorrectly assigned to the cortical bone; these objects are highlighted with a yellow circle in Fig. 2.17b. The best result for healthy patients was achieved using the threshold value of 350 Hu. For patients with osteoporosis, the threshold value of 350 Hu is too high, because the extracted cortical bone had large holes, the upper part of the cortical bone almost completely disappeared, which is highlighted in Fig. 2.17h. The best result for patients with osteoporosis was achieved using the threshold value of 250 Hu. However, as previously stated, such a threshold does not work with healthy patients. The only threshold value that was capable of extracting the cortical bone for both patient groups was 300 Hu.

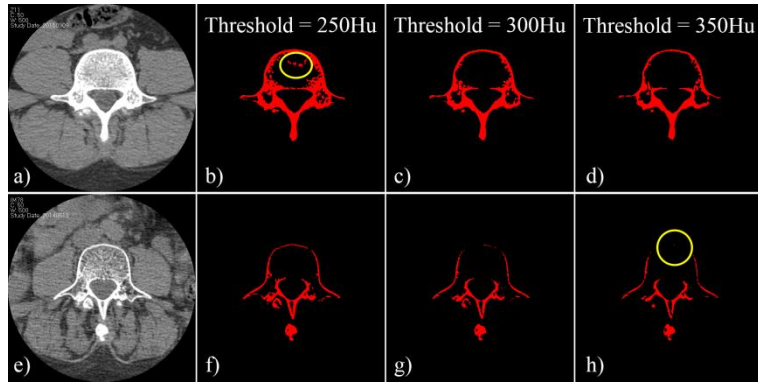


Fig. 2.17 Examples of extracted cortical bones, using different threshold values.

(The top row contains the medical images of the healthy patients, and the bottom row contains the medical images of patients with osteoporosis.)

Based on the results of the experiment, it can be concluded that by using the chosen cortical bone density threshold value, the developed algorithm has successfully managed to extract cortical and trabecular bone of the L4 vertebra from both patient groups: healthy patients and patients with osteoporosis.

The developed bone structure analysis algorithms were used to measure the cortical bone thickness and trabecular bone density of the extracted bone structures. In the next step, the average thickness (T_{avg}) and density (D_{avg}) values were calculated for each patient from all of their L4 vertebra images.

$$T_{avg} = \frac{1}{n} \sum_{i=1}^n t_i, \quad (2.10)$$

where T_{avg} — average cortical bone thickness, pixels;
 t_i — cortical bone thickness measurement on one medical image, pixels;
 n — number of images that contain the L4 vertebra.

$$D_{avg} = \frac{1}{n} \sum_{i=1}^n d_i, \quad (2.11)$$

where D_{avg} — average trabecular bone density, ratio;
 d_i — trabecular bone density measurement on one medical image, ratio;
 n — number of images that contain the L4 vertebra.

Table 2.1

Bone Structure Measurements of Healthy Patients

Patient number	Age (years)	Cortical bone average thickness (pixels)	Trabecular bone average density (ratio)
1	25	4.333	1.763
2	26	7.566	1.733
3	18	4.252	1.832
4	19	9.059	1.696
5	22	7.344	1.406
6	21	14.684	1.226
7	24	30.572	1.889
8	23	6.172	2.082
Average		7.630	1.677

Table 2.1 shows the cortical bone average thickness and trabecular bone average density measurements of eight healthy patients. The developed bone structure extraction and analysis algorithms have successfully managed to extract the bone structure and measure the cortical bone thickness trabecular bone density from the medical images of almost all eight healthy patients. The only exception, where the developed algorithms have failed, is the medical images of the 7th patient. This patient had a very high bone density and the chosen cortical bone density threshold was too small, because of that the developed algorithm incorrectly extracted some regions of the bone that could not belong to the cortical bone (see Fig. 2.18). The tissue density in this region was higher than the chosen cortical bone threshold value.

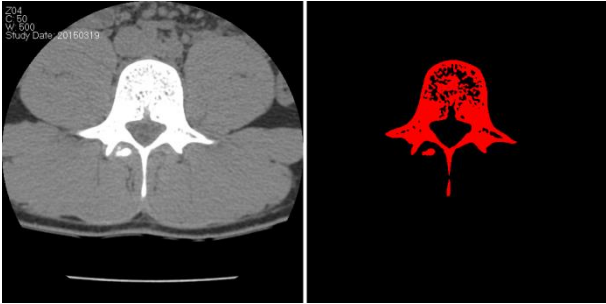


Fig. 2.18. An example of the medical image and the extracted cortical bone of the 7th patient. (The image shows that in the case of this patient the chosen cortical bone threshold value was too small.)

It was decided to exclude the measurements of the 7th patient from the average measurements of all patients. Otherwise, to correctly extract the bone structure of the 7th patient it would be necessary to increase the cortical bone threshold value, but then it would be difficult to extract the bone structure from patients with osteoporosis, whose bone density is low.

Table 2.2 shows the cortical bone average thickness and trabecular bone average density measurements of six patients with osteoporosis. The measurement results of all patients were roughly similar, with only one exception. The cortical bone average thickness of the 1st patient was significantly greater than other patients, because this patient had a tumour on the cortical bone (Fig. 2.19). Based on the results of the experiment, it can be concluded that the developed bone structure extraction algorithm is able to successfully extract the cortical and trabecular bone from both the healthy patients and patients with osteoporosis.

Table 2.2

Bone Structure Measurements of Patients with Osteoporosis

Patient number	Age (years)	Cortical bone average thickness (pixels)	Trabecular bone average density (ratio)
1	56	5.306	1.610
2	55	1.936	1.455
3	79	2.431	1.764
4	83	1.317	1.618
5	75	1.474	1.339
6	56	2.460	1.837
Average		2.487	1.604

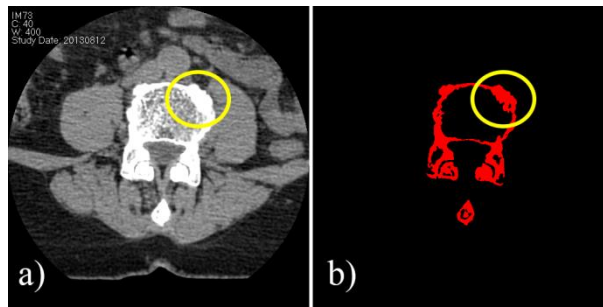


Fig. 2.19. The medical images of the 1st patient showing the tumour on the cortical bone
a) original medical image, b) processed medical image with an extracted cortical bone (the tumour is highlighted with a yellow circle).

By comparing the results of Tables 2.1 and 2.2, it can be seen that the cortical bone average thickness measurements in healthy patients are significantly higher (almost 4 times higher) than in patients with osteoporosis. However, the trabecular bone average density measurements are approximately the same for both patient groups. Based on the results of the experiment, it can be concluded that it is possible to distinguish the healthy patients from patients with osteoporosis on the basis of their cortical bone thickness measurements, which are provided by the developed bone structure analysis algorithms.

2.4.2.2 Evaluation of Changes in Bone Structure

Medical images of fifteen patients with osteoporosis were used to evaluate the changes in bone structure. Each patient had two sets of medical images, where the minimal period of time between acquiring these sets was six months. The developed algorithms were used to measure the changes in the fourth lumbar vertebra (L4). The lumbar vertebrae are the largest vertebrae of the spine, where the changes in bone structure are most visible; therefore, when radiologists analyse the spinal bone structure, they usually focus on the fourth and fifth lumbar vertebrae (the entire L4 vertebra of each patient is typically shown on 9 up to 15 medical images). Such measurements would be useful when treating patients with osteoporosis, where by analysing the changes in bone structure, it would be possible to evaluate the effectiveness of the treatment plan.

Input data: Two sets of medical images (that are stored in DICOM format) of L4 vertebra of fifteen patients (388 images in total).

Tasks:

1. To extract the cortical and trabecular bone from medical images.
2. To measure the cortical bone average thickness and trabecular bone average density.
3. To compare the results between the two sets of medical images, to determine if the developed algorithms can detect the changes in bone structure.

The developed algorithms were used to extract bone structure from each medical image of L4 vertebra and to measure the cortical bone average thickness and trabecular bone average density. The average measurement values were calculated for each set of medical images. The changes in bone structure were evaluated by comparing the measurement results between the two sets of medical images. The measurement results and the images that contain the extracted cortical and trabecular bones were saved in table in a separate document for each patient. An example of such a document can be seen in Fig. 2.20. In this example, the document consists of three pages. The table that displays the measurement results contains four columns:

1. The first column contains the original medical images of the L4 vertebra.
2. The second column contains the processed medical images from the first column that show the extracted cortical and trabecular bone.
3. The third column contains the original medical images of the L4 vertebra that were made at least six months after the images in the first column were made.

4. The fourth column contains the processed medical images from the third column that show the extracted cortical and trabecular bone.

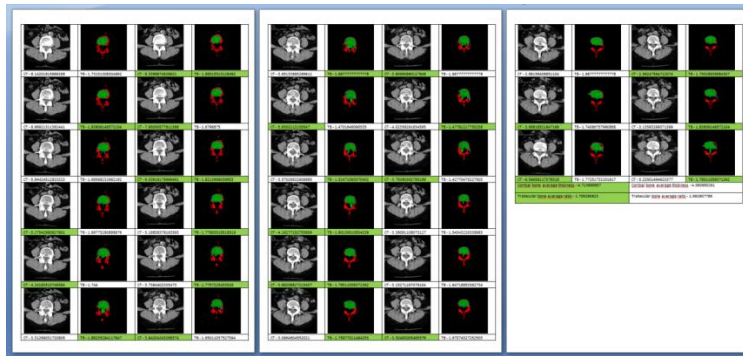


Fig. 2.20. An example of the document that contains the table with the bone structure measurement results and images of one patient.

The cortical bone thickness and trabecular bone density measurement results are inserted below the corresponding images. The average measurement results from all images are calculated at the end of the document, using formulas (2.10) and (2.11).

All the measurement results have been combined in Tables 2.3 and 2.4, where the measurement dates and results before the changes in bone structure are indicated by I, and the measurement dates and results after the changes in bone structure are indicated by II. The tables also show the time period and the difference (as a percentage) between the measurements.

Table 2.3 shows the cortical bone average thickness measurement results. The developed algorithm has been able to successfully extract the cortical bone and measure the cortical bone thickness in all the medical images of all fifteen patients.

Table 2.3

Cortical Bone Average Thickness Measurements

Patient number	The dates when the medical images were created			Cortical bone average thickness (in pixels)		
	I	II	Time period (in months)	I	II	Difference (as a percentage)
1	23.09.2013	18.03.2014	6	4.714	4.561	-3.239
2	15.01.2013	04.12.2013	11	3.330	3.020	-9.309
3	16.08.2012	06.08.2013	12	2.185	2.076	-5.005
4	26.02.2013	10.03.2014	13	5.756	5.106	-11.296
5	12.10.2011	02.09.2013	23	5.542	5.407	-2.442
6	14.02.2012	21.03.2014	25	2.577	2.394	-7.092
7	25.01.2012	14.02.2014	25	5.647	5.391	-4.530
8	18.07.2011	07.03.2014	32	4.585	3.969	-13.435
9	03.03.2011	14.02.2014	35	2.473	3.687	+32.936
10	22.03.2011	27.02.2014	35	4.109	3.750	-8.722
11	11.03.2010	29.07.2013	40	6.460	6.397	-0.978
12	12.04.2010	17.02.2014	46	4.255	3.938	-7.447
13	12.11.2008	18.07.2013	56	4.069	3.223	-20.803
14	16.02.2009	02.04.2014	62	4.674	4.545	-2.768
15	13.01.2009	29.08.2014	67	3.633	2.876	-20.833

As can be seen in Table 2.3., almost all the cortical bone average thickness measurement values decrease after the time period. The only exception is with the 9th patient,

who had developed tumour on the cortical bone after the time period, which is shown in Fig. 2.21 (the tumour is highlighted with a yellow circle); this tumour has affected the average cortical bone thickness measurement value.

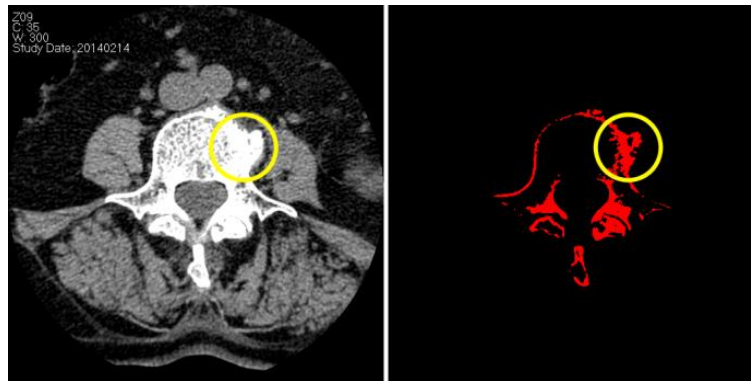


Fig. 2.21. The tumour that has grown on the cortical bone of the 9th patient.
(The tumour is highlighted with a yellow circle.)

As can be seen in Table 2.4, almost all the trabecular bone average density measurement values decrease after the time period. The measurement data from the tables have shown that bone structure measurement values always decrease with time, which corresponds to reality. This is due to the fact that the bone structure in patients with osteoporosis only deteriorates over time, and the existing treatment procedures are only able to slow down this process.

Table 2.4

Trabecular Bone Average Thickness Measurements

Patient number	The dates when the medical images were created			Trabecular bone average thickness (as a ratio)		
	I	II	Time period (in months)	I	II	Difference (as a percentage)
1	23.09.2013	18.03.2014	6	1.705	1.693	-0.744
2	15.01.2013	04.12.2013	11	1.618	1.608	-0.635
3	16.08.2012	06.08.2013	12	1.363	1.270	-6.798
4	26.02.2013	10.03.2014	13	1.803	1.627	-9.722
5	12.10.2011	02.09.2013	23	1.913	1.035	-45.891
6	14.02.2012	21.03.2014	25	1.930	1.783	-7.591
7	25.01.2012	14.02.2014	25	1.757	1.480	-15.722
8	18.07.2011	07.03.2014	32	1.732	1.638	-5.416
9	03.03.2011	14.02.2014	35	1.863	1.564	-16.057
10	22.03.2011	27.02.2014	35	1.693	1.532	-9.504
11	11.03.2010	29.07.2013	40	1.694	1.297	-23.436
12	12.04.2010	17.02.2014	46	2.194	1.678	-23.535
13	12.11.2008	18.07.2013	56	3.061	1.620	-47.079
14	16.02.2009	02.04.2014	62	2.301	1.744	-24.219
15	13.01.2009	29.08.2014	67	2.453	1.624	-33.788

Based on the results of the experiment, it can be concluded that the developed bone structure analysis algorithms are able to successfully measure the cortical bone average thickness and trabecular bone average density. The developed algorithms can be used to

monitor the changes in the cortical and trabecular bones. These measurements would be useful in the treatment of osteoporosis to determine the effectiveness of the treatment plan.

2.4.2.3 Bone Structure Visualization

Bone structure visualization can aid the diagnostic and surgery planning tasks. Medical image information can be visualized in three dimensions by creating a 3D model of the medical object.

The developed algorithms for creation and visualization of 3D models of bone structures were tested on medical images of several patients. One of the goals was to find out how the size of the marching cubes affects the quality of the surface of the 3D models. The 3D models that were created using the developed algorithm were also compared to the models created using the existing medical image processing and visualization system 3D-Doctor [33].

Creation and Visualization of a 3D Model

The developed algorithm for creating the 3D models of bone structures was tested on medical images of several patients to find out if this algorithm was capable of creating and visualizing the 3D model of L4 vertebra and the entire spine that was visible in the full set of medical images of one patient (usually it is the lower lumbar spine).

Input data: Medical images of three patients showing L4 vertebra (27 images in total) and lumbar spine (336 images in total).

Tasks: To create 3D models of one separate vertebra and lumbar spine from 2D medical images that are stored in DICOM format.

The developed algorithm has successfully managed to create six 3D models: three models of L4 vertebra (Fig. 2.22a, 2.22b, 2.22c) and three models of lumbar spine (Fig. 2.22d, 2.22e, 2.22f). In the 3D models of L4 vertebra, the cortical and trabecular bones were created as separate objects, where the cortical bone was coloured yellow and the trabecular bone — white.

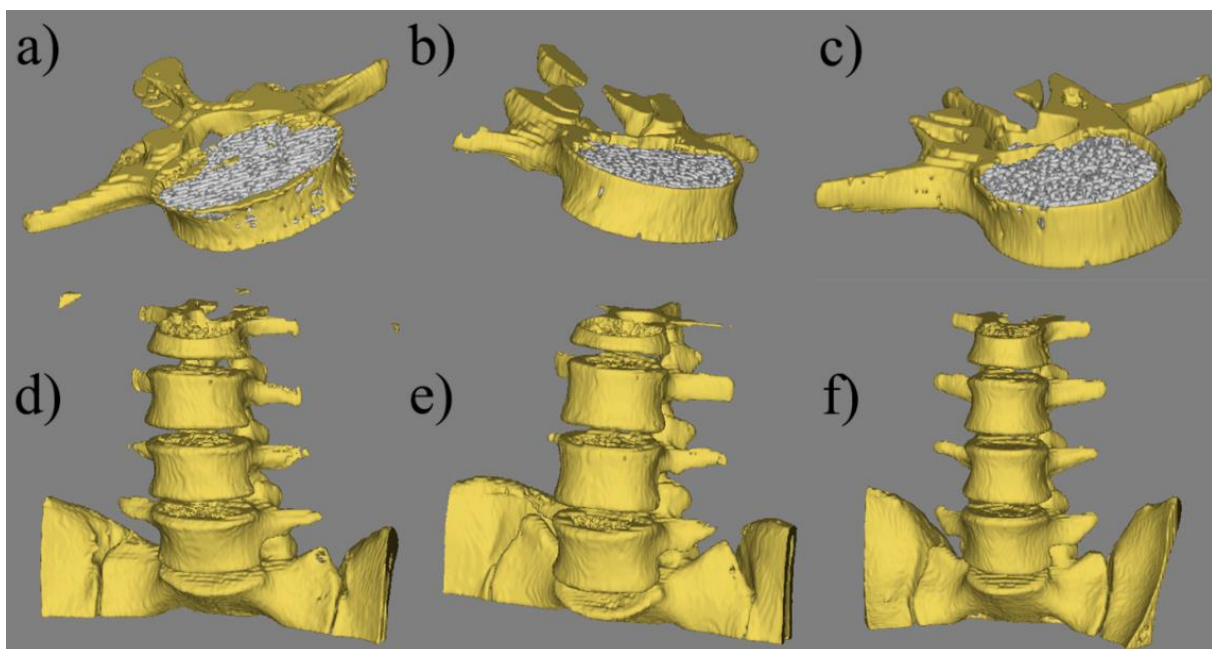


Fig. 2.22. The created 3D models of bone structures
a), b), c) 3D models of one vertebra, d), e), f), 3D models of the lumbar spine.

Based on the results of the experiment, it can be concluded that the developed algorithm, for creating and visualizing 3D models of bone structure, is able to create the 3D models of both one separate L4 vertebra and the whole lumbar spine.

Quality of the Surface of the 3D Model

The developed algorithm for creating and visualizing the 3D models of bone structures was used to create the 3D models of L4 vertebra and lumbar spine of one patient. Various marching cube sizes were used to find out how the size of the marching cubes affected the quality of the surface of the 3D model and the time it took to create it.

Input data: Medical images of one patient showing L4 vertebra (12 images in total) and lumbar spine (128 images in total).

Tasks: To create 3D models of one separate vertebra and lumbar spine from 2D medical images that are stored in DICOM format using various marching cube sizes and to compare the created 3D surfaces with each other.

The developed algorithm creates the surface of the 3D model, by dividing the medical images into cubes, where inside of each cube the 3D surface of the medical object is interpolated. The size of the marching cubes determines how many cubes will be used on one medical image. By decreasing the size of the marching cubes, the precision of the created 3D model increases, but the time it takes to create this model also increases. This happens due to the increased complexity (the 3D model contains more vertices and polygons) of the 3D model.

Four marching cube sizes were considered: 4, 3, 2 and 1 pixels. Eight 3D models were created: four L4 vertebra 3D models and four lumbar spine 3D models. Tables 2.5 and 2.6 show the number of vertices and polygons that each 3D model contains and the time it took to create each model. The created L4 vertebra and lumbar spine 3D models can be seen in Fig. 2.23.

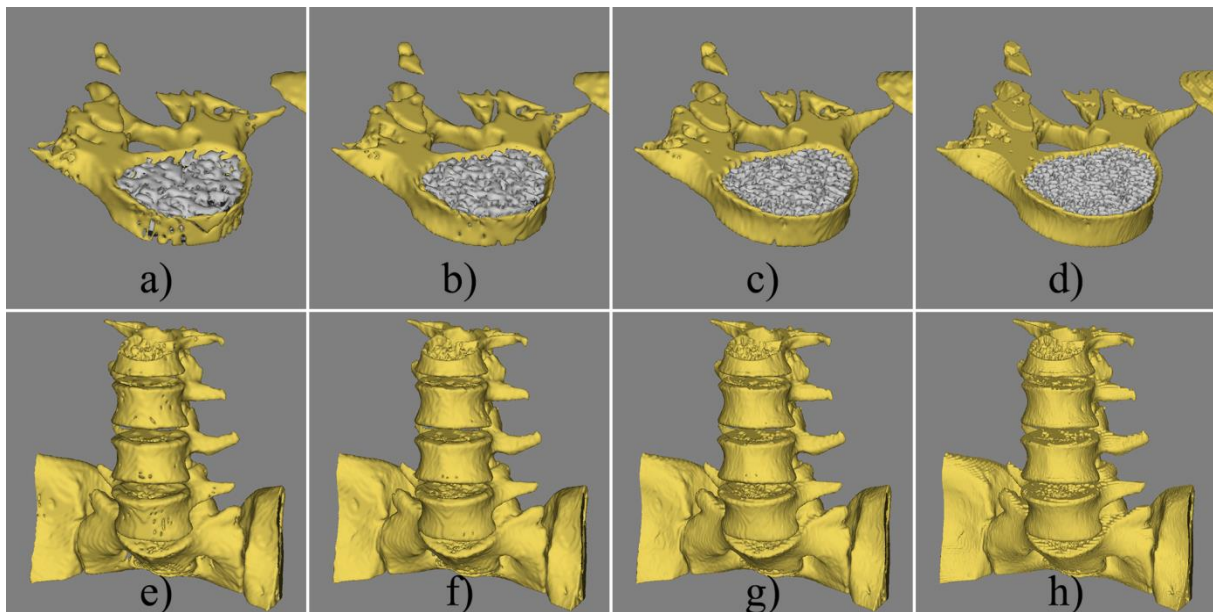


Fig. 2.23. The created 3D models of L4 vertebra and lumbar spine.

(3D models were created using the developed algorithm, using various marching cube sizes: a) and e) 4 pixels, b) and f) 3 pixels, c) and g) 2 pixels, d) and h) 1 pixel.)

Table 2.5

Statistics of 3D Models of L4 Vertebra

Marching cube size (in pixels)	Cortical bone		Trabecular bone		3D model creation time (in seconds)
	Vertex count	Polygon count	Vertex count	Polygon count	
4	12823	25637	11811	18115	2.431
3	19584	39079	18222	32603	2.984
2	36112	72103	33537	62095	4.852
1	111161	222241	100164	170435	22.178

As can be seen in Table 2.5, the time it took to create the 3D models using marching cube sizes of 3 and 4 pixels is quite small (less than three seconds) and almost the same, when compared to the other 3D models. However, looking at the created 3D models (Fig. 2.23a and 2.23b), it can easily be seen that the created 3D surface imprecisely describes the medical object, because it contains several holes that are not visible on more precise 3D model (Fig. 2.23d), which was made using the smallest possible marching cube size — 1 pixel. The differences between the 3D surfaces that were created using marching cube sizes of 2 and 1 pixels are minimal (Fig. 2.23c and 2.23d), but the creation time differs significantly. The 3D model that was acquired using marching cube size of 2 pixels was created almost four times faster than the 3D model that was created using marching cube size — 1 pixel. Therefore, it can be concluded that the best marching cube size for creating 3D models of L4 vertebra is 2 pixels. However, it would be more appropriate to use the smallest size (1 pixel), since it provides maximum precision of the 3D surface, and precision is very important in medicine.

As can be seen in Table 2.6, the time it took to create the 3D models of lumbar spine is very different among all marching cube sizes. Looking at the created 3D models (Fig. 2.23), it can be seen that the 3D models that were created using the marching cube size of 4 and 3 pixels (Fig. 2.23e and 2.23f) imprecisely describe the medical objects in the same way as the 3D models of L4 vertebra, since they contain holes that are not visible in a more precise 3D model (Fig. 2.23h), which was made using the smallest possible marching cube size — 1 pixel. The time it took to create the 3D model that most precisely describes the medical object (Fig. 2.23h), using marching cube size of 1 pixel, was the longest out of all the models. Therefore, it can be concluded that in the case of 3D model of lumbar spine, it is better to use the marching cube size of 2 pixels, since the creation time is significantly faster (161 seconds) and differences between the created 3D surfaces are minimal (Fig. 2.23g and 2.23h).

Table 2.6

Statistics of 3D Models of Lumbar Spine

Marching cube size (in pixels)	Cortical bone		3D model creation time (in seconds)
	Vertex count	Polygon count	
4	160143	318191	75.538
3	243918	485009	96.773
2	442806	883453	161.005
1	1291863	2583131	595.841

Comparing the Developed Algorithm with Another Method

The 3D model that was created using the developed algorithm was compared with a 3D model that was created using the existing medical image processing and visualization system 3D-Doctor [33].

Input data: Two sets of medical images of lumbar spine of two patients (128 and 121 images in total).

Tasks: To create 3D models of lumbar spine from 2D medical images that are stored in DICOM format, using the developed algorithm and the 3D-Doctor system, and to compare the results.

The developed algorithm was used to create 3D models of the lumbar spine of two patients, using the marching cube sizes — 2 and 1 pixels. The 3D-Doctor system was used to create the 3D models of lumbar spine for the same two patients, using the same medical images. The created 3D models of lumbar spine can be seen in Fig. 2.24.

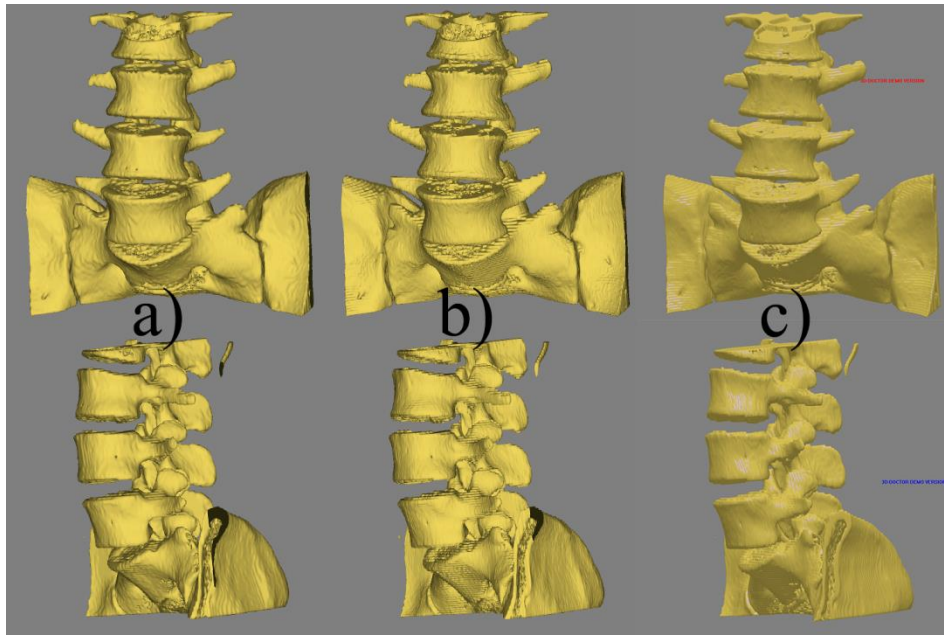


Fig. 2.24. The created 3D models of lumbar spine

a) the result of the developed algorithm (marching cube size — 2 pixels), b) the result of the developed algorithm (marching cube size — 1 pixel), c) the result of the 3D-Doctor system.

As can be seen in Fig. 2.24, the staircase effect to a different extent appears on all models (the staircase effect is highlighted with red circles in Fig. 2.25). The staircase effect appears in the regions between the medical images that the 3D models are based on and the strength of this effect depends on the distance between the medical images and the 3D model surface smoothing algorithm.

The surface of the 3D model, which was created using the developed algorithm with marching cube size of 1 pixel, is similar to the 3D model that was created using the 3D-Doctor system. Both these models have the distinct staircase effect in the same places. But, the 3D model with the smoothest surface was the one created by using the developed algorithm with marching cube size of 2 pixels (Fig. 2.25a).

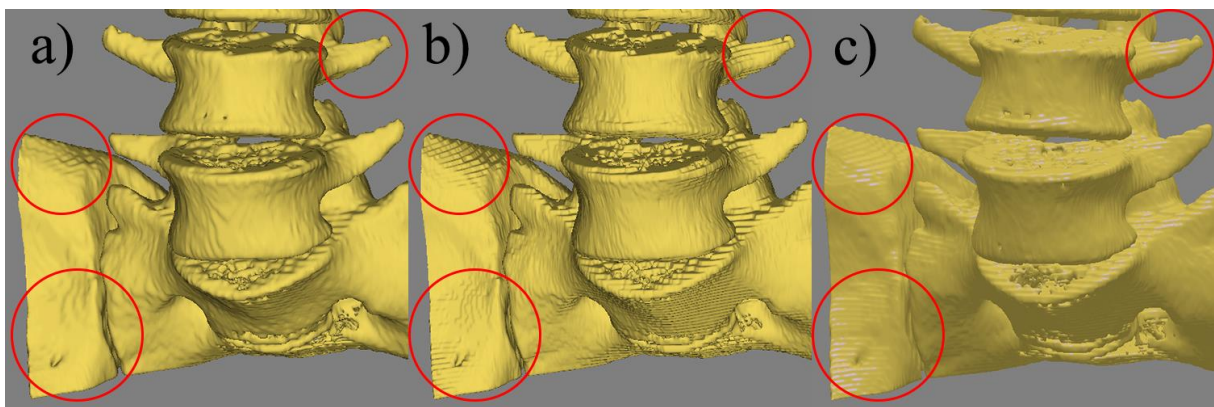


Fig. 2.25. The staircase effect on the surface of the 3D models

a) the result of the developed algorithm (marching cube size — 2 pixels), b) the result of the developed algorithm (marching cube size — 1 pixel), c) the result of the 3D-Doctor system.

2.5. Results and Conclusions

The bone structure analysis and visualization in this Thesis are based on medical images that were acquired using computed tomography. Medical image analysis is a topical issue; recently many new methods of analysing medical images have been developed using the

information technologies for various medical objects and tasks. Bone structure analysis is needed to determine bone strength and assess the damage to the bone micro-architecture that appears due to such bone disease as osteoporosis.

Various medical imaging methods, existing medical images processing methods and methods for creating 3D models of medical objects have been analysed and examined in this Thesis. Most existing medical image processing algorithms are manual or semi-automatic algorithms. When using such algorithms, a physician has to intervene in the medical image segmentation process, to set or edit the segmentation parameters or manually define the approximate borders of segments. The existing methods have been found to have the following disadvantages:

1. Manual extraction of a region of interest from the medical image, when compared to a traditional or an automatic medical image analysis, takes more time and requires additional software and experience when working with it, so typically it is not performed in clinical practice. To speed up this process, it is desirable to develop fully automatic methods; however, the manual intervention often is necessary to correct the errors of an automated algorithm.
2. Manual analysis of medical images is very subjective, because it depends on human perception and produces variable measurements. To acquire more objective, reproducible measurements, it is necessary to perform the appropriate image processing methods and computational strategies that are based on the data from the medical images.
3. Most of the examined medical image segmentation methods use images that were acquired using high resolution medical imaging devices, which are not available in ordinary hospitals and diagnostic centres.

Modern information technologies can aid the diagnostic and surgery planning tasks. Medical image information can be visualized in three dimensions by creating a 3D model of the medical object. 3D models of the spine could be used in orthopaedic surgical planning, vertebral body compression, osteoporotic or pathological fractures, in cases of spinal canal or intervertebral stenosis, vertebral arch and joint spur pathology.

There are many methods that are used to create 3D models. Most popular visualization method in the medical field is volume rendering. One of the disadvantages of volume rendering is that it requires a considerable amount of computational resources, which are not available in most computers. Another visualization method is surface rendering, this method requires less computational resources, but surface rendering has its own disadvantages. For example, triangulation algorithms are meant for solid objects and they are unable to create a polygonal surface for porous objects such as the cortical and the trabecular bone. Surface rendering methods that are based on the marching cube algorithm can create a polygonal surface for any object; however, the created surface has a distinct aliasing effect and the surface is not smooth.

All the above-mentioned medical image processing methods are usually combined into one medical image processing system. There are several systems, which contain various tools for medical image processing and analysis. However, such systems are usually integrated into special workstations connected to the medical imaging equipment (computed tomography, magnetic resonance imaging, etc.). There are also systems, which could be installed on any computer; however, such systems, usually only allow viewing the medical images and do not contain the necessary medical image analysis tools.

The aforementioned disadvantages create the need to develop new medical image processing methods and combine them in one system that would not have these disadvantages. Therefore, the goal of the Thesis has been to develop methods, which can be used for bone structure analysis and automatically evaluate changes in bone structure after a time period. The following tasks have been solved in the Thesis:

1. New medical image processing methods have been developed, which can work with images stored in DICOM format. The developed program can also open DICOMDIR files that can contain many DICOM images of different patients.
2. New methods have been developed for extracting the bone structure from medical images. The developed methods are capable of extracting the cortical and trabecular bones from medical images. The extraction process is fully automatic; however, the operator has the option of editing the main parameters to increase the precision of the extraction algorithm.
3. New methods of evaluating the changes in bone structure have been developed. The developed methods can automatically measure the cortical bone average thickness and the trabecular bone average density.
4. New bone structure 3D visualization methods have been developed. The developed methods are based on the marching cube algorithm and are capable of creating the 3D models of cortical and trabecular bones. The marching cube algorithm was modified by adding the options to smooth the 3D surface of the objects and visually display the thickness of the cortical bone.

The developed methods for bone structure extraction and analysis work completely automatically and process a single medical image faster than 1 second. As a result, they produce an image with an extracted bone structure and measurement results. This process is faster than the traditional medical image analysis, where the radiologist visually looks through all the medical images that are divided into slices. Furthermore, with the help of the developed methods that are based on the defined bone structure extraction parameters, it is possible to achieve reproducible measurements, which would be useful when analysing the bone structure of patients with osteoporosis.

The developed methods for cortical bone average thickness, porosity and trabecular bone average density would be useful to physicians that are treating patients with osteoporosis. The developed methods allow assessing the dynamic changes in bone structure and evaluating the effectiveness of treatment.

The developed methods for bone structure 3D visualization can create the 3D models of the cortical and trabecular bone automatically based on the data from the medical images. The created models can be rotated, scaled and looked at from all the possible angles; this could aid the diagnostic and surgery planning tasks.

Various experiments have been conducted to test the effectiveness of the developed algorithms. The experiments have been meant to test if the developed algorithms are able to successfully extract the bone structure from medical images and if they can be used to evaluate the changes in bone structure. It has also been tested if the developed algorithms are able to create and visualize the 3D models of bone structure. Based on the results of the experiments, it can be concluded that the developed bone structure extraction algorithm is capable of extracting the bone structure from both the healthy patients and patients with osteoporosis. The developed bone structure analysis algorithms have successfully managed to measure the cortical bone average thickness and the trabecular bone average density. It has been concluded that the developed algorithms can be used to evaluate changes in the cortical and trabecular bones. By using the developed algorithms, it is possible to distinguish the healthy patients from patients with osteoporosis based on their cortical bone thickness measurements. The developed bone structure 3D model creation and visualization algorithm has also been compared with the existing medical image processing and visualization system 3D-Doctor [33], and it has been concluded that the 3D model created by the developed algorithm has better quality (smoother) 3D surface.

All the developed algorithms have been approbated by attending the scientific conferences and the experimental results have been published in scientific publications. Further studies can be performed to expand the statistics of using the algorithm of evaluating the changes in bone structure with more patients with bone structures in various states. The

measurement results of the developed algorithm can also be compared with the results of DXA (dual-energy X-ray absorptiometry) analysis, which currently is the traditional method that is used to diagnose and monitor osteoporosis in clinical practice.

3. REFERENCES

- [1] Bhalerao A., Wilson R. Unsupervised Image Segmentation Combining Region and Boundary Estimation // *Image and Vision Computing*, Volume 19, Issue 6, 15 April 2001, pp. 353–368.
- [2] Chao W. H., Chen Y. Y., Lin S. H., Shih Y. Y. I., Tsang S.. Automatic Segmentation of Magnetic Resonance Images Using a Decision Tree with Spatial Information // *Computerized Medical Imaging and Graphics*, Volume 33, Issue 2, March 2009, pp. 111–121.
- [3] Cheng H.D., Jiang X.H., Sun Y., Wang J. Color Image Segmentation: Advances and Prospects // *Pattern Recognition*, Volume 34, Issue 12, December 2001, pp. 2259–2281.
- [4] Elnagar A., Alhaji R.. Segmentation of Connected Handwritten Numeral Strings // *Pattern Recognition*, Volume 36, Issue 3, March 2003, pp. 625–634.
- [5] Kurugollu F., Sankur B., Harmanci A. Emre. Image Segmentation by Relaxation Using Constraint Satisfaction Neural Network // *Image and Vision Computing*, Volume 20, Issue 7, 1 May 2002, pp. 483–497.
- [6] McGuinness K., O'Connor N. E. A Comparative Evaluation of Interactive Segmentation Algorithms // *Pattern Recognition*, Volume 43, Issue 2, February 2010, pp. 434–444.
- [7] Melton L. J., Atkinson E. J., O'Connor M. K., et al. Bone Density and Fracture Risk in Men // *Journal of Bone and Mineral Research*, Volume 13, 1998, pp. 1915–1923.
- [8] Pichel J. C., Singh D. E., Rivera F. F. Image Segmentation Based on Merging of Sub-optimal Segmentations // *Pattern Recognition Letters*, Volume 27, Issue 10, 15 July 2006, pp. 1105–1116.
- [9] Udupa J. K., LeBlanc V. R., Zhuge Y., Imielinska C., Schmidt H., Currie L. M., Hirsch B. E., Woodburn J. A Framework for Evaluating Image Segmentation Algorithms // *Computerized Medical Imaging and Graphics*, Volume 30, Issue 2, March 2006, pp. 75–87.
- [10] Zhang H., Fritts J. E., Goldman S. A. Image Segmentation Evaluation: A Survey of Unsupervised Methods // *Computer Vision and Image Understanding*, Volume 110, Issue 2, May 2008, pp. 260–280.
- [11] Zouagui T., Benoit-Cattin H., Odet C. Image Segmentation Functional Model // *Pattern Recognition*, Volume 37, Issue 9, September 2004, pp. 1785–1795.
- [12] Bueno G., Musse O., Heitz F., Armspach J. P., Three-Dimensional Segmentation of Anatomical Structures in MR Images on Large Data Bases // *Magnetic Resonance Imaging*, Volume 19, Issue 1, January 2001, pp. 73–88.
- [13] Dastidar P., Heinonen T., Numminen J., Rautiainen M., Laasonen E. Semi-automatic Segmentation of Computed Tomographic Images in Volumetric Estimation of Nasal Airway // *European Archives of Oto-Rhino-Laryngology*, Volume 256, Number 4, 1999, pp. 192–198.
- [14] van Ginneken B., Stegmann M. B., Loog M. Segmentation of Anatomical Structures in Chest Radiographs Using Supervised Methods: A Comparative Study on a Public Database // *Medical Image Analysis*, Volume 10, Issue 1, February 2006, pp. 19–40.
- [15] Worth A. J., Kennedy D. N. Segmentation of Magnetic Resonance Brain Images Using Analogue Constraint Satisfaction Neural Networks // *Image and Vision Computing*, Volume 12, Issue 6, July-August 1994, pp. 345–354.
- [16] Boutroy S., Bouxsein M. L., Munoz F., Delmas P. D. In Vivo Assessment of Trabecular Bone Microarchitecture by High-Resolution Peripheral Quantitative Computed

- Tomography // *The Journal of Clinical Endocrinology and Metabolism*, Vol. 90, 2005, pp. 6508–6515.
- [17] Buie H. R., Campbell G. M., Klinck R. J., et al. Automatic Segmentation of Cortical and Trabecular Compartments Based on a Dual Threshold Technique for in Vivo Micro-CT Bone Analysis // *Bone*, Vol. 41, 2007, pp. 505–515.
- [18] Burghardt A. J., Link T. M., Majumdar S. High-Resolution Computed Tomography for Clinical Imaging of Bone Microarchitecture // *Clinical Orthopaedics and Related Research*, Vol. 469, 2011, pp. 2179–2193.
- [19] Hyun B, Newitt D. C., Majumdar S. Assessment of Cortical Bone Structure Using High-Resolution Magnetic Resonance Imaging // *Proceedings of the 13th Scientific Meeting, International Society for Magnetic Resonance in Medicine*, Miami, 7–13 May 2005.
- [20] Krug R., Burghardt A. J., Majumdar S., Link T. M. A High-Resolution Imaging Techniques for the Assessment of Osteoporosis // *Radiologic Clinics of North America*, Vol. 48, 2010, pp. 601–621.
- [21] Cohen I., Gordon D. VS: A Surface-Based System for Topological Analysis, Quantization and Visualization of Voxel Data // *Medical Image Analysis*, Volume 13, Issue 2, April 2009, pp. 245–256.
- [22] Huppertz H. J., Grimm C., Fauser S., Kassubek J., Mader I., Hochmuth A., Spreer J., Schulze-Bonhage A. Enhanced Visualization of Blurred Gray–White Matter Junctions in Focal Cortical Dysplasia by Voxel-Based 3D MRI Analysis // *Epilepsy Research*, Volume 67, Issues 1–2, October–November 2005, pp. 35–50.
- [23] Levoy M. Display of Surfaces from Volume Data // *IEEE Computer Graphics and Applications*, Volume 8, 1988, pp. 29–37.
- [24] Li G., Xie H., Ning H., Capala J., Arora B. C., Coleman C. N., Camphausen K., Miller R. W. A Novel 3D Volumetric Voxel Registration Technique for Volume-View-Guided Image Registration of Multiple Imaging Modalities // *International Journal of Radiation Oncology*Biophysics*, Volume 63, Issue 1, 1 September 2005, pp. 261–273.
- [25] Vesanto J. SOM-Based Data Visualization Methods // *Intelligent Data Analysis*, Volume 3, Issue 2, August 1999, pp. 111–126.
- [26] Wu Y. From CT Image to 3D Model // *Advanced Imaging*, August 2001, pp. 20–23.
- [27] Zaharia M. D., Dorst L. Modeling and Visualization of 3D Polygonal Mesh Surfaces Using Geometric Algebra // *Computers & Graphics*, Volume 28, Issue 4, August 2004, pp. 519–526.
- [28] Boločko K., Kovaļovs M., Glazs A. Medical Image 3D Visualization by Vector Based Methods // *Multi Conference on Computer Science and Information Systems, Computer Graphics, Visualization, Computer Vision and Image Processing (IADIS): Proceedings*, Italy, Rome, 24–26 July 2011.
- [29] Kovaļovs M., Glazs A. Par vienu pieeju medicīnas attēlu 3D modeļa izstrādāšana// *RTU Zinātniskie raksti, 5. sērija. Datorzinātne. 42. sējums. Datorvadības tehnoloģijas*, Rīga, Latvija, 2010, 19–23 lpp.
- [30] Sisojevs A., Kovaļovs M., Glazs A. Medical Object 3D Visualization Method Based on the Bézier Triangles // *Multi Conference on Computer Science and Information Systems, Computer Graphics, Visualization, Computer Vision and Image Processing (IADIS): Proceedings*, Portugal, Lisbon, 21–23 July 2012, pp. 185–187.
- [31] Lorensen W. E., Cline H. E. Marching Cubes: A High Resolution 3D Surface Reconstruction Algorithm// *Proceedings of the 14th Annual Conference on Computer Graphics and Interactive Techniques, SIGGRAPH*, Volume 21, 1987,–pp. 163–169.
- [32] Nielson G. M., Hamann B. The Asymptotic Decider: Resolving the Ambiguity in Marching Cubes // *Proceedings of the 2nd Conference on Visualization '91*, 1991.
- [33] Able Software Corp. 3D-Doctor, FDA 510K Cleared, Vector-Based 3D Imaging, Modeling and Measurement Software. –Available at <http://www.ablesw.com/3d-doctor/index.html>

- [34] Hendee W. R. *Medical Imaging Physics*. 4th Edition. New York: John Wiley & Sons, 2003, 536 p.
- [35] Röntgen W. *Über eine neue Art von Strahlen // Annalen der Physik*, Volume 300, 1898, pp. 12–17.
- [36] Glaser, O. *Evolution of Radiologic Physics as Applied to Isotopes // American Journal of Roentgenology, Radium Therapy*, Volume 65, 1951, 515 p.
- [37] Laughlin, J. *History of Medical Physics // Encyclopaedia of Medical Devices and Engineering*, Vol. 3. New York: John Wiley & Sons, 1988, 1878 p.
- [38] Wong A., Lou S. L. *Medical Image Archive, Retrieval, and Communication // Handbook of Medical Image Processing and Analysis (Second Edition)*. Waltham, Massachusetts: Academic Press, 2009, pp. 861–873.
- [39] Bushberg J. T., Seibert J. A., Leidholdt Jr. E. M., Boone J. M. *The Essential Physics of Medical Imaging (2nd Edition)*. Philadelphia: Lippincott Williams & Wilkins, 2001, 933 p.
- [40] Suetens P. *Fundamentals of Medical Imaging (2nd Edition)*. New York: Cambridge University Press, 2009, 253 p.
- [41] Kelsey A. C., Heintz H. P., Sandoval J. D. et al. *Radiation Biology of Medical Imaging*. Hoboken, New Jersey: John Wiley & Sons, 2014, 315 p.
- [42] Hounsfield, G. *Computerized Transverse Axial Scanning (Tomography): Part I. Description of System // The British Journal of Radiology*, Volume 46, 1973,– pp. 1016–1022.
- [43] Ledley R., DiChiro G., Lussenhop A., et al. *Computerized Transaxial X-Ray Tomography of the Human Body // Science*, Volume 186, 1974, pp. 207–212.
- [44] Hendee, W. *Physical Principles of Computed Tomography*. Boston: Little Brown&Co., 1983, 192 p.
- [45] Hounsfield G. N. *Computed Medical Imaging // Medical Physics*, Volume 7, 1980, pp. 283–290.
- [46] Bloch F., Hansen W., Packard M. *The Nuclear Induction Experiment // Physical Review*, Volume 70, 1946, pp. 474–485.
- [47] Bloch F. *Nuclear Induction // Physical Review*, Volume 70, –1946, pp. 460–473.
- [48] Lauterbur P. *Image Formation by Induced Local Interactions: Examples Employing Nuclear Magnetic Resonance // Nature*, Volume 242, 1973, pp. 190–191.
- [49] Garroway A. N., Grannell P. K., Mansfield P. *Image Formation in NMR by a Selective Irradiative Process // Journal of Physics C: Solid State Physics*, Volume 7, 1974, pp. 457–462.
- [50] Einstein A. *Zur Elektrodynamik bewegter Körper // Annalen der Physik*, Volume 322, 1905, pp. 891–921.
- [51] Bottomley P. A., Foster T. H., Argersinger R. E., et al. *A Review of Normal Tissue Hydrogen NMR Relaxation Times and Relaxation Mechanisms from 1–100 MHz: Dependence on Tissue Type, NMR Frequency, Temperature, Species, Excision, and Age // Medical Physics*, Volume 11, 1984, pp. 425–448.
- [52] Hinshaw W. S. *Image Formation by Nuclear Magnetic Resonance: The Sensitive Point Method // Journal of Applied Physiology*, Volume 47, 1976, pp. 3709–3721.
- [53] Andrew E. R., Bottomley P. A., Hinshaw W. S., et al. *NMR Images by the Multiple Sensitive Point Method: Application to Larger Biological Systems // Physics in Medicine and Biology*, Volume 22, 1977, pp. 971–974.
- [54] Hinshaw W. S. *Spin Mapping: The Application of Moving Gradients to NMR // Physics Letters A*, Volume 48, 1974, pp. 87–88.
- [55] Mansfield P., Maudsley A. A. *Medical imaging by NMR// The British Journal of Radiology*. - 1977. - Volume 50. - 188–194 lpp.
- [56] Lauterbur P. C. *Image Formation by Induced Local Interactions: Examples Employing Nuclear Magnetic Resonance // Nature*, Volume 242, 1973, pp. 190–191.

- [57] Kumar A., Welti I., Ernst, R. R. NMR Fourier Zeugmatography // *Journal of Magnetic Resonance*, Volume 18, 1975, pp. 69– 83.
- [58] Graff K. F. Ultrasonics: Historical Aspects // *Ultrasonics Symposium Proceedings*, 1977, pp. 1–10.
- [59] Hendeel W. R., Holmes J. H. History of Ultrasound Imaging // *Medical Physics of CT and Ultrasound*. New York: American Institute of Physics, 1980, 717 p.
- [60] Hendeel W. R. Cross Sectional Medical Imaging: A History // *Radiographics*, Volume 9, 1989, pp. 1155–1180.
- [61] McDicken W. Diagnostic Ultrasonics. New York: John Wiley & Sons, 1976, 248 p.
- [62] Tatarinov A. M., Egorov V. P., Sarvazyan A. P. The Dual-Frequency Method for Ultrasonic Assessment of Skeletal System // *Acoustical Physics*, Volume 55, 2009, pp. 665–673.
- [63] Gregg E. W., Kriska A. M., Salamone L. M., et al. The Epidemiology of Quantitative Ultrasound: A Review of the Relationships with Bone Mass, Osteoporosis and Fracture Risk // *Osteoporosis International*, Volume 7, –1997, pp. 89–99.
- [64] Tuna H., Birtane M., Ekuklu G., et al. Does Quantitative Tibial Ultrasound Predict Low Bone Mineral Density Defined by Dual Energy X-Ray Absorptiometry? // *Yonsei Medical Journal*, Volume 49, 2008, pp. 436–442.
- [65] National Electrical Manufacturers Association: DICOM Standard Website. Accessed at <http://dicom.nema.org/>
- [66] American Society for Bone and Mineral Research: Bone Structure and Function– Accessed at <http://depts.washington.edu/bonebio/ASBMRed/structure.html>
- [67] Hernlund E., Svedbom A., Ivergard M, et al. Osteoporosis in the European Union: Medical Management, Epidemiology and Economic Burden. A report prepared in collaboration with the International Osteoporosis Foundation (IOF) and the European Federation of Pharmaceutical Industry Associations (EFPIA) // *Archives of Osteoporosis*, Volume 8, Article 136, 2013, 115 p.
- [68] Kanis J. A., Johnell O., Oden A., et al. Long-Term Risk of Osteoporotic Fracture in Malmö // *Osteoporosis International*, Volume 11, 2000, pp. 669–674.
- [69] Melton L. J., Chrischilles E. A., Cooper C., et al. Perspective. How Many Women Have Osteoporosis? // *Journal of Bone and Mineral Research*, Volume 7, 1992, pp. 1005–1010.
- [70] Adams J. E. Dual-Energy X-Ray Absorptiometry // *Radiology of Osteoporosis*, Medical Radiology. Berlin: Springer, 2008, pp. 105–124.
- [71] Ammann P., Rizzoli R. Bone Strength and Its Determinants // *Osteoporosis International*, Volume 14, 2003, pp. 13–18.
- [72] Chapurlat R. D., Delmas P. D. Bone Microdamage: A Clinical Perspective // *Osteoporosis International*, Volume 20, 2009, pp. 1299–1308.
- [73] Seeman E., Delmas P. D. Bone Quality—The Material and Structural Basis of Bone Strength and Fragility // *The New England Journal of Medicine*, Volume 354, 2006, pp. 2250–2261.
- [74] Black D. M., Thompson D. E. The Effect of Alendronate Therapy on Osteoporotic Fracture in the Vertebral Fracture Arm of the Fracture Intervention Trial // *International Journal of Clinical Practice*. Supplement, Volume 101, 1999, pp. 46–50.
- [75] Marshall D., Johnell O., Wedel H.. Meta-Analysis of How Well Measures of Bone Mineral Density Predict Occurrence of Osteoporotic Fractures // *BMJ*, 1996; 312, pp. 1254–1259.
- [76] Wehrli F. W., Saha P. K., Gomberg B. R., et al. Role of Magnetic Resonance for Assessing Structure and Function of Trabecular Bone // *Topics in Magnetic Resonance Imaging*, Volume 13, 2002, pp. 335–355.
- [77] Hildebrand T., Laib A., Muller R., et al. Direct Three-Dimensional Morphometric Analysis of Human Cancellous Bone: Microstructural Data from Spine, Femur, Iliac Crest,

- and Calcaneus // *Journal of Bone and Mineral Research*, Volume 14, 1999, pp. 1167–1174.
- [78] Bousson V., Peyrin F., Bergot C., et al. Cortical Bone in the Human Femoral Neck: Three-Dimensional Appearance and Porosity Using Synchrotron Radiation // *Journal of Bone and Mineral Research*, Volume 19, 2004, pp. 794–801.
- [79] Lai C. C., Chang C. Y. A Hierarchical Evolutionary Algorithm for Automatic Medical Image Segmentation // *Expert Systems with Applications*, Volume 36, Issue 1, January 2009, pp. 248–259.
- [80] Navon E., Miller O., Averbuch A. Color Image Segmentation Based on Adaptive Local Thresholds // *Image and Vision Computing*, Volume 23, Issue 1, 1 January 2005, pp. 69–85.
- [81] Taheri S., Ong S. H., Chon V. F. H. Level-Set Segmentation of Brain Tumors Using a Threshold-Based Speed Function // *Image and Vision Computing*, Volume 28, Issue 1, January 2010, pp. 26–37.
- [82] Carvalho E. A., Ushizima D. M., Medeiros F. N. S., Martins C. I. O., Marques R. C. P., Oliveira I. N. S. SAR Imagery Segmentation by Statistical Region Growing and Hierarchical Merging // *Digital Signal Processing*, Volume 20, Issue 5, September 2010, pp. 1365–1378.
- [83] Sandor T., Metcalf D., Kim Y. J.. Segmentation of Brain CT Images Using the Concept of Region Growing // *International Journal of Bio-Medical Computing*, Volume 29, Issue 2, November 1991, pp. 133–147.
- [84] He L., Peng Z., Everding B., Wang X., Han C. Y., Weiss K. L., Wee W. G. A Comparative Study of Deformable Contour Methods on Medical Image Segmentation // *Image and Vision Computing*, Volume 26, Issue 2, 1 February 2008, pp. 141–163.
- [85] Wang L., Li C., Sun Q., Xia D., Kao C. Y. Active Contours Driven by Local and Global Intensity Fitting Energy with Application to Brain MR Image Segmentation // *Computerized Medical Imaging and Graphics*, Volume 33, Issue 7, October 2009, pp. 520–531.
- [86] Adams R., Bischof L. Seeded Region Growing // *IEEE Transactions on Pattern Analysis and Machine Intelligence*, Volume 16, 1994, pp. 641–647.
- [87] Brice C. R., Fenema C. L. Scene Analysis Using Regions // *Artificial Intelligence*, Volume 1, 1970, pp. 205–226.
- [88] Chang Y. L., Li X. Adaptive Image Region-Growing // *IEEE Transactions on Image Processing*, Volume 3, 1994, pp. 868–872.
- [89] Hojjatoleslami S. A., Kittler J. Region Growing: A New Approach // *IEEE Transactions on Image Processing*, Volume 7, 1998, pp. 1079–1084.
- [90] Wan S. Y., Higgins W. E. Symmetric Region Growing // *IEEE Transactions on Image Processing*, Volume 12, 2003, pp. 1007–1015.
- [91] Pratt W. K. *Digital Image Processing: PIKS Scientific Inside*, 4th Edition. Hoboken, New Jersey: John Wiley & Sons, 2007, 782 p.
- [92] Foley D. J., van Dam A., Feiner K. S., Hughes F. J. *Computer Graphics: Principles and Practice in C (2nd Edition)*. Boston: Addison-Wesley, 1995, 1175 p.
- [93] Gouraud H. Continuous Shading of Curved Surfaces // *IEEE Transactions on Computers*, Volume C-20, 1971, pp. 623–629.
- [94] Phong B. T. Illumination for Computer Generated Pictures // *Communications of the ACM*, Volume 18, 1975, pp. 311–317.
- [95] Suetens P., Fua P., Hanson A. J. Computational Strategies for Object Recognition // *ACM Computing Surveys*. Volume 24, 1992, pp. 5–61.
- [96] Kovalovs M., Platkajis A. Analysis of the Treatment Effectiveness for Osteoporosis by Using Images, Acquired by Computer Tomography // *Proceedings of the 9th Baltic-Bulgarian Conference on Bionics and Prosthetics Biomechanics and Mechanics Mechatronics and Robotics*, Riga, Latvia, 17–18 June 2013, pp. 215–218.

- [97] Kovalovs M., Glazs A. The Cortical and Trabecular Bone Extraction from Medical Images to Determine the Effectiveness of Treatment of Osteoporosis // Biomedical Engineering Conference Proceedings. Kaunas University of Technology, Kaunas, Lithuania, 25–26 October 2012, pp. 103–106.
- [98] Kovaļovs M., Glazs A. Medical Image Analysis to Determine the Effectiveness of Osteoporosis Treatment // Scientific Journal of RTU Technologies of Computer Control, Volume 13. Riga: RTU, 2012, pp. 11–14.
- [99] Kovaļovs M., Glazs A. Trabecular Bone Segmentation by Using an Adaptive Contour // RTU Scientific Proceedings, Technologies of Computer Control, No. 14, 2013, pp. 6–11.
- [100] Kovalovs M., Glazs A. Automatic Medical Image Analysis for Measuring Bone Thickness and Density // Conference Biomedical Engineering Proceedings. Kaunas University of Technology, Kaunas, Lithuania, 27–28 November 2014, pp. 153–157.
- [101] Kovalovs M., Glazs A. Automatic Medical Image Analysis for Measuring Cortical Bone Porosity // Biomedical Engineering Conference Proceedings. Kaunas University of Technology, Kaunas, Lithuania, 28–29 November 2013, pp. 87–90.
- [102] Kovaļovs M., Glazs A. Medicīnisko objektu virsmu modelēšana, izmantojot triangulācijas un maršējošo kubu algoritmu // RTU Zinātniskie raksti, 5. sērija. Datorzinātne. 48.sējums Datorvadības tehnoloģijas, Rīga, Latvija, 2011, 25-29 lpp.
- [103] Jain A. Fundamentals of Digital Image Processing. New Jersey: Prentice-Hall, 1989, 565 p.
- [104] Kovaļovs M., Glazs A., 3D Visualization of Bone Structure and Thickness // RTU Scientific Proceedings, Technologies of Computer Control, No. 15, 2014, pp. 20–26.